Coordinated Planning for Multiple Inner Networks of Offshore Wind Farms and Onshore Transmission Expansion

Yutao Liang, Shunjiang Lin, *Senior Member*, *IEEE*, Xin Lai, Mingbo Liu, *Member*, *IEEE*, and Binrui Zhang

***Abstract*—A mismatch between the rapid growth of grid-connected offshore wind farms (OWFs) and the delay of onshore transmission expansion (OTE) planning has caused significant wind curtailment in power systems. To alleviate this problem, a coordinated planning (CP) model of multiple inner networks of OWFs (INOWFs) and OTE is established in this paper. In the proposed CP model, the explicit connection topology constraints of a new double-sided ring topology for INOWFs are defined, and the connection topologies and electrical components of both INOWFs and OTE are coordinately optimized. In addition, a parallel random search method is proposed to obtain the set of feasible connection topology schemes of each INOWF, which can contract the feasible region of the CP model and reduce the difficulty in obtaining the optimal solution. Finally, a decomposition and coordination planning algorithm is developed to decompose the original complex optimization model into two tractable sub-models for INOWF and OTE planning. This approach efficiently obtains the optimal CP scheme for multiple INOWFs and OTE through alternating iterations. Case studies on the modified IEEE 39-bus system with two OWFs and an actual provincial power system with six OWFs demonstrate the correctness and efficiency of the proposed model and algorithm.**

***Index Terms*—Coordinated planning, decomposition and coordination optimization, offshore wind farm, parallel random search, transmission expansion planning.**

Received: May 29, 2024
Accepted: August 12, 2024
Published Online: May 1, 2025

Yutao Liang, Shunjiang Lin (corresponding author), Xin Lai, and Mingbo Liu are with the School of Electric Power Engineering, and the Guangdong Key Laboratory of Clean Energy Technology, South China University of Technology, Guangzhou 510640, China (e-mail: 291611021@qq.com; linshj@scut.edu.cn; 2770726188@qq.com; epmbliu@scut.edu.cn).

Binrui Zhang is with the China Nuclear Power Engineering Co., Ltd., Shenzhen 518124, China (e-mail: zhangbinrui@cgnpc.com.cn).

DOI: 10.23919/PCMP.2024.000078

NOMENCLATURE

A. Sets and Indices

$i/j/i'/j'$	indices of buses
$ij/i'j'$	indices of transmission corridors or submarine cables
w/s	index of WTs/candidate offshore or onshore substations
k/Ω_{cc}	index/set of types of collector submarine cables
h/Ω_{ct}	index/set of types of transmission submarine cables
p/Ω_{TR}	index/set of types of transformers
m/Ω_{F}	index/set of OWFs
n/Ω_{PCC}	index/set of candidate PCCs for OWFs
Ω_{L}	set of onshore transmission corridors
$\Omega_{G}/\Omega_{Ld}/\Omega_{RE}$	set of buses of thermal power units/loads/ existing renewable energy stations in OTN
Ω_{Lc}/Ω_{Lt}	set of collector/transmission submarine cables
Ω_{wt}	set of buses of WTs in OWFs
Ω_{Bc}/Ω_{Bt}	set of buses in the OWF collector/ transmission system
$\Omega_{s}^{off}/\Omega_{s}^{on}$	set of buses of candidate offshore/onshore substations in OWF

B. Parameters

T_{a}	number of hours in a year, i.e., 8760 h
r/T_{l}	discount rate/service life of OWFs, i.e., 8%/25 a
C_{Bij}	investment cost per unit length of transmission corridor ij
$C_{Ld}/C_{RE}/C_{PR}$	load shedding cost/renewable energy curtailment cost of existing renewable energy stations/OWF feed-in tariff
L_{ij}	distance between bus i to j
$L_{inv.c}/L_{inv.t}$	investment limit of the total length of collector/transmission submarine cables
$P_{REi\,max}$	maximum active power output of existing renewable energy station at bus i

R_{th}/g_{th} resistance/conductance per unit length of the hth type of transmission submarine cables

$R_{ck}/g_{ck}/b_{ck}$ resistance/conductance/susceptance per unit length of the kth type of collector submarine cables

$Q_{Gi,l}/M_{Gi,l}$ slope/intercept of the lth segment of the piecewise linear cost function of the thermal power unit at bus i

C_{th} investment cost per unit length of the hth type of transmission submarine cables

C_{si} transportation and installation cost of submarine cables

$\alpha_a/\beta_a/\gamma_a$ cost parameters of AC submarine cables

$I_{n,k/h}(S_{sz})$ current-carrying capacity of the kth/hth type of AC submarine cables depending on cross-sectional area S_{sz}

α_d/β_d cost parameters of DC submarine cables

$P_{n,h}$ rated power of the hth type of DC submarine cables

$S_{TN,p}$ rated capacity of the pth type of single transformer

φ_{cv} power factor angle of the converter

x_{ij}^0 number of existing lines of transmission corridor ij

$N_{ij\max}$ maximum number of lines in transmission corridor ij

P_{Li}/Q_{Li} active/reactive load power at bus i

g_{ij}/b_{ij} conductance/susceptance of single line in transmission corridor ij

$P_{ij\max}^s/Q_{ij\max}^s$ maximum active/reactive transmission power of single line in transmission corridor ij

$\theta_{ij\min}/\theta_{ij\max}$ minimum/maximum phase angle difference between buses i and j

M a large constant

$q_{\max}$ maximum network flow

$\omega_{\min}/\omega_{\max}$ minimum/maximum topological redundancy of the INOWF

n_L total number of possible connections of submarine cables

$N_{\min}^{PCC}/N_{\max}^{PCC}$ minimum/maximum number of PCCs for each OWF

$N_{SC,\min}/N_{SC,\max}$ minimum/maximum number of offshore substations

$N_{Fc,\min}/N_{Fc,\max}$ minimum/maximum number of collector feeders

$N_{Ft,\min}/N_{Ft,\max}$ minimum/maximum number of transmission feeders

$x_{i(j)}/y_{i(j)}$ horizontal/ordinate coordinate of bus $i(j)$

$x_{i'(j')}/y_{i'(j')}$ horizontal/ordinate coordinate of bus $i'(j')$

λ minimum wind power utilization rate

$P_{\Sigma n}$ total installed capacity of OWF at PCC n

$P_{v,\min}^{ac}/P_{v,\max}^{ac}$ minimum/maximum value of P_{si}^{ac}

$Q_{v,\min}^{ac}/Q_{v,\max}^{ac}$ minimum/maximum value of Q_{si}^{ac}

γ/U_N^c margin coefficient/rated voltage

φ_{ij}/φ_s power factor angle of submarine cable ij/ substation s

$P_{wi\min}/P_{wi\max}$ minimum/maximum active power output of WT w at bus i

$\varphi_{w\min}/\varphi_{w\max}$ minimum/maximum power factor angle of WT w

$U_{i\min}^{c(t)}/U_{i\max}^{c(t)}$ minimum/maximum voltage magnitude of bus i on the collector (transmission) side

$\theta_{ij\min}^c/\theta_{ij\max}^c$ minimum/maximum phase angle difference between buses i and j in the OWF collector system

m_t binary parameter indicating whether the DC transmission mode is adopted

C. Variables

C_{op} annual operation cost of OTN

$C_{in}/C_{lo}/C_{wc}$ annual equivalent investment/power loss/wind curtailment cost of OWFs

$C_{c,ij}/C_{t,ij}$ investment cost of collector/transmission submarine cable ij.

$C_{sc,s}^{off}/C_{sc,s}^{on}$ investment cost of offshore/onshore substation s

x_{ij} number of newly-built lines for transmission corridor ij

F_{Gi} generation cost of the thermal power unit at bus i

$\Delta P_{Li}/\Delta Q_{Li}$ active/reactive load shedding power at bus i

P_{REi}/Q_{REi} injected active/reactive power of existing renewable energy station at bus i

$u_{ij(ji)}^c/u_{ij(ji)}^t$ binary variable indicating whether the collector/transmission submarine cable is connected from bus $i(j)$ to $j(i)$

$u_{i'j'(j'i')}^c$ binary variable indicating whether the collector submarine cable is connected from bus $i'(j')$ to $j'(i')$

$u_{is(sj)}^c/u_{is(sj)}^t$ binary variable indicating whether the collector/transmission submarine cable is connected from bus $i(s)$ to $s(j)$

u_{kij}^c/u_{kji}^c binary variable indicating whether the kth type of collector submarine cables is connected from bus i to j/bus j to i

u_{hij}^t/u_{hji}^t binary variable indicating whether the hth type of transmission submarine cables is connected from bus i to j/bus j to i

P_{ij}^{c}/Q_{ij}^{c}	active/reactive power of collector submarine cable *ij*
P_{ij}^{t}/Q_{ij}^{t}	active/reactive power of transmission submarine cable *ij*
$\tilde{I}_{ij}^{t}$	square of current magnitude of transmission submarine cable *ij*
P_{Gi}/Q_{Gi}	injected active/reactive power of thermal power unit at bus *i*
$C_{T,s}/C_{SG,s}/C_{P,s}$	transformer cost/switching equipment cost on the collector side/offshore platform construction cost of substation *s*
$C_{cv,s}/C_{eq,s}$	converter equipment cost/matching electrical equipment cost of substation *s*
$z_s/z_{p,s}$	binary variable indicating whether the candidate substation *s*th/*p*th type transformer in substation *s* is selected
u_{ij}	binary variable indicating whether there is a connection of transmission corridor from bus *i* to *j*
$P_{ni}^{PCC}/Q_{ni}^{PCC}$	injected active/reactive power of OWF PCC *n* at bus *i* of OTN
P_{ij}/Q_{ij}	active/reactive power of transmission corridor *ij* in OTN
$U_{i(j)}/\theta_{i(j)}$	voltage magnitude/phase angle of bus *i*(*j*) in OTN
P_{ij}^{s}/Q_{ij}^{s}	active/reactive power of single line in transmission corridor *ij*
q_i/q_{Li}	injected flow/load flow at bus *i*
$q_{ij(ji)}$ / q_{ii}	network flow from bus *i*(*j*) to *j*(*i*)/ network flow output at bus *i*
ω	topological redundancy of the INOWF
z_n	binary variable indicating whether the OWF selects PCC *n*
P_i^{c}/Q_i^{c}	injected active/reactive power at bus *i* in the collector system
$U_{i(j)}^{c}/\theta_{i(j)}^{c}$	voltage magnitude/phase angle of bus *i*(*j*) in the collector system
P_i^{t}	injected active power at bus *i* in the OWF transmission system
U_i^{t}/U_j^{t}	voltage magnitude of bus *i*/bus *j* in the OWF transmission system
P_{si}^{ac}/Q_{si}^{ac}	active/reactive power injection or output at the AC bus *i* of the VSC station *s*
P_{si}^{dc}	active power injection or output at the DC bus *i* of the VSC station *s*
U_s^{ac}/U_s^{dc}	voltage magnitude on the AC/DC side in the VSC station *s*
P_{wi}/Q_{wi}	active/reactive power output of WT *w* at bus *i*
θ_{ref}^{c}	phase angle of the reference bus in the OWF collector system
n_{ijm}	auxiliary binary variable of x_{ij}
$\boldsymbol{h}_1/\boldsymbol{h}_2/\boldsymbol{h}_3$	constraint vectors

I. Introduction

Offshore wind power generation has become an important research direction in the development of low-carbon power systems due to its advantages of high wind energy density, stable wind speed, and large single-unit capacity. In recent years, global investment and construction of offshore wind farms (OWFs) have experienced rapid growth. The installed global offshore wind power capacity is expected to reach 270 GW by 2030 and 2000 GW by 2050 [1], [2]. The inner network of an OWF (INOWF) consists of the collector system, offshore substations, transmission system and onshore substations, which work together to collect and transmit wind power. The OWF is connected to the onshore transmission network (OTN) through the points of common coupling (PCCs) [3], [4]. The INOWF planning and the onshore transmission expansion (OTE) planning are closely connected through PCCs and are mutually influenced by the coupling of electrical quantities at the PCCs. Therefore, the mismatch between the rapid growth of OWFs and the delay of OTE planning can cause severe transmission bottlenecks, leading to large-scale wind power curtailment and loss of benefits for the OWFs and OTN. For instance, in Germany, an OWF with an installed capacity of 276 MW was delayed in integration in 2018 because of the weakness of the coastal OTN [5]. Thus, addressing the coordinated planning (CP) problem of multiple INOWFs and OTE is crucial and requires an urgent solution.

To improve the investment economics and operational reliability of OWFs, numerous studies have focused on the optimal planning of INOWFs [6]–[13], whereas the planning of OWF collector systems has also been studied in [6]–[10]. In [6] and [7], a bi-level multi-objective optimization framework considering the joint optimization of wind turbine (WT) micro-siting and the radial topology is proposed to obtain an optimal OWF layout that could maximize the wind power output while minimizing the cable cost. In [8], a method for the optimization of the number of offshore substations and their locations is proposed to obtain an optimal connection topology of an OWF. In [9] and [10], the explicit constraints of the double-sided ring (DSR) topology are constructed, and an optimal planning model is proposed to obtain the optimal DSR topology to reduce the investment cost and improve the reliability of an OWF. On the other hand, the planning of OWF transmission systems has also been studied in [11]–[13]. In [11], a method is developed to obtain the optimal design and configuration of the OWF transmission system including the optimal voltage level and the optimal number of reactors and their location. In [12], an offshore transmission network planning model considering a variety of uncertainties is proposed for large-scale wind power integration to select the best transmission mode. In [13], the economics and reliability of OWF transmission systems with different high-voltage direct current configurations are evaluated, and the topology is planned using the particle swarm optimization method. However, most existing studies

have focused only on the planning of a single OWF's collector or transmission system without considering the interaction between the planning processes of a collector and a transmission system. In addition, with the OWF development toward a large-scale, clustering, and deep-sea direction, new technologies including new DSR topology with cross-substation incorporation (CSI) [14], voltage source converter based multi-terminal high-voltage direct current (VSC-MTDC) transmission mode [15], design to merge offshore step-up and converter substations with overlapping functions [16], and the planning considering multiple PCCs [17], have been proposed. These advanced OWF grid-connected technologies can further improve the economics and reliability of OWFs and promote the accommodation of wind power. Moreover, OWFs are usually located at the end of the OTN, leading to a weak connection. Therefore, the transmission lines close to the PCCs in an OTN need to be expanded to meet the requirements of large-scale wind power transmission. However, the existing studies on INOWF planning have been conducted independently of OTE planning. Thus, to improve the benefits of the overall planning scheme, it is necessary to plan multiple INOWFs and OTE coordinately, considering the advanced OWF grid-connected technologies for INOWF planning.

To meet the increasing load demand, the coordinated generation and transmission planning problems have been studied [18]–[20]. In [18], a stochastic adaptive robust optimization method is proposed to solve generation and transmission expansion planning problems while minimizing the expansion and operation costs. In [19] and [20], a CP model is constructed to plan generators, transmission lines and reactive power compensation equipment. However, the aforementioned studies focus on CP of conventional generators and the transmission network without considering OWF planning. Moreover, with the rapid development of OWFs, many studies have discussed the OTE planning with multiple OWFs [21]–[26]. In [21], a CP method for large-scale INOWFs and associated regional transmission networks is proposed to reduce wind power curtailment, and a bi-level model is expressed as a linearized mathematical problem with equilibrium constraints. In [22] and [23], a CP model of OWFs, energy storage, and a transmission system, considering optimal transmission switching and unit commitment, is constructed to accommodate renewable energy. In [24], the expansion planning scheme of a wind farm-integrated power system is obtained by considering multiple flexibility sources and using affine policies to enhance the flexibility of the power system in response to uncertain variations of the net system demand. In [25] and [26], an OTE optimization model considering the load and wind power uncertainties is proposed to determine the optimal number of expanded lines and the optimal OWF capacity. However, in [21]–[26], an OWF is regarded as a variable injected power into the PCC limited by its total installed capacity. This simplified method cannot accurately reflect the impact of OWFs' inner topology and electrical component planning on the OTN, resulting in low economics of the obtained planning solution. Therefore, the CP of multiple INOWFs and OTE requires further research. Furthermore, planning multiple INOWFs and OTE at the same time can increase the scale of variables and constraints of the CP problem, so the centralized solution method is no longer applicable. Thus, how to contract the feasible region and decompose the entire problem is the key to efficiently solving the CP model.

The main contributions of this paper are twofold:

1) A CP model of multiple INOWFs and OTE, which considers investment economics and operational reliability, is constructed. In this model, explicit connection topology constraints of INOWFs, considering the new DSR topology with CSI, are defined. The planning also coordinate the topologies of INOWFs, the type of AC/DC submarine cables, the site and capacity of offshore/onshore substations, the number of feeders connected to offshore/onshore substations, the grid-connected PCCs, and the expansion of onshore transmission lines.

2) To solve the proposed CP model, a parallel random search (PRS) method is introduced to obtain feasible connection topology schemes of each INOWF. This approach helps contract the feasible region and reduce the solution complexity. In addition, a decomposition and coordination planning (DCP) algorithm is proposed, which decomposes the original complex model into two tractable sub-models of INOWF planning and OTE planning for alternating iteration solution to obtain the optimal CP scheme, with significantly improved computational efficiency.

The rest of this paper is organized as follows. Section II describes the CP problem, while Section III introduces a CP model of multiple INOWFs and OTE. Section IV proposes a PRS method and a DCP algorithm to solve the proposed CP model. Section V presents the case studies on the modified IEEE 39-bus system and an actual provincial power system. Finally, Section VI presents the conclusions.

II. Problem Description

The schematic diagram of the CP of multiple INOWFs and OTE is presented in Fig. 1. The electrical structure of an INOWF mainly includes five parts: offshore WTs, collector system, offshore substations (offshore step-up substation or step-up converter substation), transmission system, and onshore substations (onshore switching substation or converter substation). Similarly, the electrical structure of an OTN mainly includes the PCCs of OWFs, substations, and transmission corridors. This paper studies the CP problem of multiple INOWFs and OTE. For the INOWF, the topologies of collector and transmission systems, the types of AC and DC submarine cables, the number/capacity/location of offshore and onshore substations, the number of collector and transmission feeders connected to offshore and onshore substations, and the number/location of PCCs are optimized. For the OTN, the expansion of transmission lines is optimized.

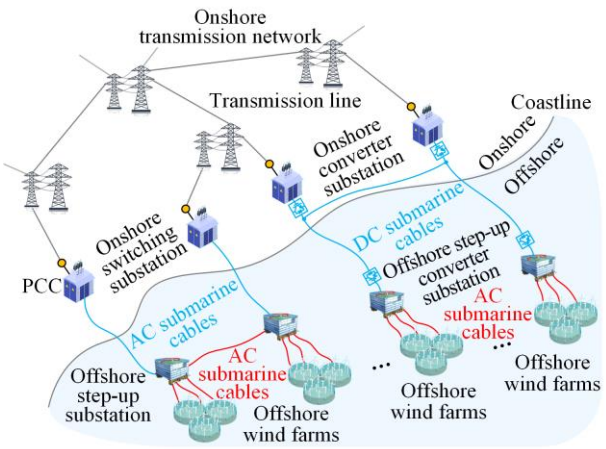

Fig. 1. Schematic diagram of the CP of multiple INOWFs and OTE.

The CP of multiple INOWFs and OTE is a complex problem, and several simplifications and assumptions are adopted based on actual OWF projects as follows: 1) The micro-siting of WTs is determined through aerodynamic and site characteristics, and it is assumed that the number and locations of WTs are known. 2) The OWF AC collector and VSC-MTDC transmission system merge at the offshore step-up and converter substations, so only the offshore step-up converter substation is planned. 3) Each offshore (onshore) substation is equipped with two transformers with the same capacity. 4) The offshore (onshore) substation's sites and PCC locations for each OWF are selected and optimized from the limited candidate site sets. 5) The INOWF topology optimization considers the new DSR topology with CSI [14]. 6) The voltage levels of the OWF collector and transmission systems are fixed. 7) If an OWF's offshore distance exceeds 40 km, the grid-connected mode of AC collector and VSC-MTDC transmission is adopted. If an OWF's offshore distance is less than 40 km, the grid-connected mode of AC collector and AC transmission is adopted. In summary, combined with the actual OWF projects, the simplifications 1), 3), 4), 6), and 7) are adopted to reduce the complexity of the CP problem of multiple INOWFs and OTE, and the assumptions 2) and 5) are adopted to consider the advanced OWF grid-connected technologies for further improving the economics and reliability of INOWF planning.

III. Coordinated Planning Model

Considering the investment economics and operational reliability, a CP model for multiple INOWFs and OTE is proposed. The main object is to minimize the total annual equivalent investment and operation cost of the entire system.

A. Objective Function

The total annual equivalent investment and operation cost of the CP model consists of the expansion planning cost of OTN and the planning cost of INOWFs, as given in (1). Among them, the expansion planning cost of OTN includes the annual equivalent expansion investment cost of newly-built transmission lines and the annual operation cost consisting of the thermal power units' generation cost, load shedding cost, and renewable energy curtailment cost of existing renewable energy stations, as shown in (2). The planning cost of INOWFs includes their annual equivalent investment cost, network power loss cost and wind curtailment cost, as shown in (3), while the investment cost consists of the costs of collector and transmission submarine cables and the offshore and onshore substations.

$$\min f_{\mathrm{TE}} + \sum\nolimits_{m\in\Omega_{\mathrm{F}}} f_{\mathrm{OWF},m} \tag{1}$$

$$\begin{cases} f_{\mathrm{TE}} = r(1+r)^{T_{\mathrm{i}}} \Big/ \left[(1+r)^{T_{\mathrm{i}}} - 1\right] \times \\ \qquad \sum\nolimits_{ij\in\Omega_{\mathrm{L}}} C_{\mathrm{B}ij} L_{ij} x_{ij} + C_{\mathrm{op}} \\ C_{\mathrm{op}} = T_{\mathrm{a}} \left[\begin{array}{l} \sum\nolimits_{i\in\Omega_{\mathrm{G}}} F_{\mathrm{G}i} + \sum\nolimits_{i\in\Omega_{\mathrm{Ld}}} C_{\mathrm{Ld}} \Delta P_{\mathrm{L}i} + \\ \sum\nolimits_{i\in\Omega_{\mathrm{RE}}} C_{\mathrm{RE}} (P_{\mathrm{RE}i\max} - P_{\mathrm{RE}i}) \end{array} \right] \end{cases} \tag{2}$$

$$\begin{cases} f_{\mathrm{OWF},m} = C_{\mathrm{in}} + C_{\mathrm{lo}} + C_{\mathrm{wc}} \\ C_{\mathrm{in}} = \dfrac{r(1+r)^{T_{\mathrm{i}}}}{(1+r)^{T_{\mathrm{i}}} - 1} \left(\begin{array}{l} \sum\nolimits_{ij\in\Omega_{\mathrm{Lc}}} C_{\mathrm{c},ij} + \sum\nolimits_{ij\in\Omega_{\mathrm{Lt}}} C_{\mathrm{t},ij} + \\ \sum\nolimits_{s\in\Omega_{\mathrm{s}}^{\mathrm{off}}} C_{\mathrm{sc},s}^{\mathrm{off}} + \sum\nolimits_{s\in\Omega_{\mathrm{s}}^{\mathrm{on}}} C_{\mathrm{sc},s}^{\mathrm{on}} \end{array} \right) \\ C_{\mathrm{lo}} = C_{\mathrm{PR}} T_{\mathrm{a}} \sum\nolimits_{ij\in\Omega_{\mathrm{Lc}}} \left[\sum\nolimits_{k\in\Omega_{\mathrm{cc}}} (u_{kij}^{\mathrm{c}} + u_{kji}^{\mathrm{c}}) R_{\mathrm{c}k} \right] \times \\ \qquad L_{ij} \left[(P_{ij}^{\mathrm{c}})^2 + (Q_{ij}^{\mathrm{c}})^2 \right] + C_{\mathrm{PR}} T_{\mathrm{a}} \times \\ \qquad \sum\nolimits_{ij\in\Omega_{\mathrm{Lt}}} \left[\sum\nolimits_{h\in\Omega_{\mathrm{ct}}} (u_{hij}^{\mathrm{t}} + u_{hji}^{\mathrm{t}}) R_{\mathrm{t}h} \right] L_{ij} \tilde{I}_{ij}^{\mathrm{t}} \\ C_{\mathrm{wc}} = C_{\mathrm{RE}} T_{\mathrm{a}} \sum\nolimits_{i\in\Omega_{\mathrm{wt}}} \left(P_{wi\max} - P_{wi} \right) \end{cases} \tag{3}$$

where if AC transmission is adopted, $\tilde{I}_{ij}^{\mathrm{t}} = (P_{ij}^{\mathrm{t}})^2 + (Q_{ij}^{\mathrm{t}})^2$; and if DC transmission is adopted, $\tilde{I}_{ij}^{\mathrm{t}} = (P_{ij}^{\mathrm{t}})^2$. The calculation of power losses ignores the influence of voltage.

$F_{\mathrm{G}i}$ in (2) is a quadratic function of $P_{\mathrm{G}i}$, which is piecewise linearized to obtain the convex inequalities[27]:

$$F_{\mathrm{G}i} \geqslant Q_{\mathrm{G}i,l} P_{\mathrm{G}i} + M_{\mathrm{G}i,l}, \quad l = 1, 2, \cdots \tag{4}$$

The AC submarine cable cost is related to the voltage level, length, and current-carrying capacity while the DC submarine cable cost is related to the voltage level, length, and rated power. Thus, the investment costs of collector and transmission submarine cables in (3) are shown in (5) and (6) [11], [28]. The investment costs of offshore and onshore substations under AC and DC transmission modes are different, including the transformer cost, switching equipment cost, offshore platform construction cost, converter equipment cost and matching electrical equipment cost, which is related to the transformer capacity and the number of feeders, as shown in (7) [8].

$$C_{\mathrm{c},ij} = \sum\nolimits_{k\in\Omega_{\mathrm{cc}}} L_{ij} \left(C_{\mathrm{si}} + \alpha_{\mathrm{a}} + \beta_{\mathrm{a}} \mathrm{e}^{\gamma_{\mathrm{a}} 10^{-5} I_{\mathrm{n},k} S_{\mathrm{sz}}} \right) \left(u_{kij}^{\mathrm{c}} + u_{kji}^{\mathrm{c}} \right) \tag{5}$$

$$C_{\mathrm{t},ij} = \sum\nolimits_{h\in\Omega_{\mathrm{ct}}} L_{ij} C_{\mathrm{t}h} \left(u_{hij}^{\mathrm{t}} + u_{hji}^{\mathrm{t}} \right) \tag{6}$$

$$\begin{cases} C_{\mathrm{sc},s}^{\mathrm{off}} = C_{\mathrm{T},s} + C_{\mathrm{SG},s} + C_{\mathrm{P},s} + m_{\mathrm{t}} C_{\mathrm{cv},s} + C_{\mathrm{eq},s} \\ C_{\mathrm{sc},s}^{\mathrm{on}} = m_{\mathrm{t}} C_{\mathrm{cv},s} + C_{\mathrm{eq},s} \\ C_{\mathrm{T},s} = \sum\nolimits_{p\in\Omega_{\mathrm{TR}}} 242.602 \times (2S_{\mathrm{TN},p})^{0.7513} z_{p,s} \\ C_{\mathrm{SG},s} = 3266.96 \left(\sum\nolimits_{i\in\Omega_{\mathrm{Bc/t}}} u_{is}^{\mathrm{c/t}} + \sum\nolimits_{j\in\Omega_{\mathrm{Bc/t}}} u_{sj}^{\mathrm{c/t}} \right) \\ C_{\mathrm{P},s} = \sum\nolimits_{p\in\Omega_{\mathrm{TR}}} \left(15595.678 + 544.391 \times 2S_{\mathrm{TN},p} \right) z_{p,s} \\ C_{\mathrm{cv},s} = \sum\nolimits_{p\in\Omega_{\mathrm{TR}}} 1352.9 \cos\varphi_{\mathrm{cv}} \times 2S_{\mathrm{TN},p} z_{p,s} \\ C_{\mathrm{eq},s} = 300000 z_s \end{cases} \tag{7}$$

where if AC transmission is adopted, $C_{th}=C_{si}+\alpha_a+\beta_a e^{\gamma_a 10^{-5} I_{n,h} S_{sz}}$ and m_t equals zero; If DC transmission is adopted, $C_{th}=\alpha_d+\beta_d P_{n,h}$ and m_t equals one.

B. Constraints of OTN

1) Expansion Constraints of Transmission Corridors

The OTE includes two situations: new transmission corridors are built, and new transmission lines in the existing transmission corridors are built. The number of lines in each transmission corridor is limited, as shown in (8). Since x_{ij} is an integer variable, to facilitate subsequent processing of non-convex constraints and reduce the number of binary variables, x_{ij} is expressed in the binary form as shown in (9). When $u_{ij}=0$, $x_{ij}^0+x_{ij}=0$, indicating that there is no transmission corridor between buses i and j; when $u_{ij}=1$, $1\leqslant x_{ij}^0+x_{ij}\leqslant N_{ij\max}$, indicating that the transmission corridor between buses i and j has at least one transmission line.

$$u_{ij}\leqslant x_{ij}^0+x_{ij}\leqslant N_{ij\max}u_{ij},\ u_{ij}\in\{0,1\} \tag{8}$$

$$x_{ij}=\sum_{m=0}^{M_L}2^m n_{ijm},\ n_{ijm}\in\{0,1\},\ m=0,1,\cdots,M_L \tag{9}$$

where M_L is a given non-negative integer, and it satisfies $N_{ij\max}\leqslant 2^{M_L+1}-1$.

2) Network Security Constraints

In the OTN, the power balance equation constraints of bus i are shown as:

$$\begin{cases}P_{Gi}+P_{ni}^{PCC}+P_{REi}-\left(P_{Li}-\Delta P_{Li}\right)=\sum_{j\in i}P_{ij}\\ Q_{Gi}+Q_{ni}^{PCC}+Q_{REi}-\left(Q_{Li}-\Delta Q_{Li}\right)=\sum_{j\in i}Q_{ij}\end{cases} \tag{10}$$

Based on the linear power flow equations in [29], the security constraints of transmission corridors are shown in (11)–(14). Equation (11) is the power flow constraint of a single line in the transmission corridor ij; equation (12) is the transmission capacity constraint of a single line in the transmission corridor ij; equation (13) is the formula for calculating the transmission power of transmission corridor ij; and (14) is the voltage phase angle constraint of two end buses of transmission corridor ij.

$$\begin{cases}P_{ij}^s=g_{ij}\left(U_i-U_j\right)-b_{ij}\left(\theta_i-\theta_j\right)\\ Q_{ij}^s=-b_{ij}\left(U_i-U_j\right)-g_{ij}\left(\theta_i-\theta_j\right)\end{cases} \tag{11}$$

$$\begin{cases}-P_{ij\max}^s-M\left(1-u_{ij}\right)\leqslant P_{ij}^s\leqslant P_{ij\max}^s+M\left(1-u_{ij}\right)\\ -Q_{ij\max}^s-M\left(1-u_{ij}\right)\leqslant Q_{ij}^s\leqslant Q_{ij\max}^s+M\left(1-u_{ij}\right)\end{cases} \tag{12}$$

$$\begin{cases}P_{ij}=\left(x_{ij}^0+x_{ij}\right)P_{ij}^s=x_{ij}^0P_{ij}^s+\sum_{m=0}^{M_L}2^m n_{ijm}P_{ij}^s\\ Q_{ij}=\left(x_{ij}^0+x_{ij}\right)Q_{ij}^s=x_{ij}^0Q_{ij}^s+\sum_{m=0}^{M_L}2^m n_{ijm}Q_{ij}^s\end{cases} \tag{13}$$

$$-M\left(1-u_{ij}\right)+\theta_{ij\min}\leqslant\theta_i-\theta_j\leqslant M\left(1-u_{ij}\right)+\theta_{ij\max} \tag{14}$$

3) Upper and Lower Bound Constraints of Variables

The upper and lower bound constraints of variables include the active and reactive power of thermal power units and existing renewable energy stations, the active and reactive load shedding power, and the bus voltage, shown as:

$$\boldsymbol{\chi}_{\min}\leqslant\boldsymbol{\chi}\leqslant\boldsymbol{\chi}_{\max} \tag{15}$$

where $\boldsymbol{\chi}=\left(P_{Gi},Q_{Gi},P_{REi},Q_{REi},\Delta P_{Li},\Delta Q_{Li},U_i\right)$.

C. Constraints of INOWFs

1) Connection Topology Constraints

Compared with the traditional DSR, the new DSR with CSI can achieve capacity sharing between different substations while maintaining the advantage of high reliability of the ring topology [14], as shown in Fig. 2. Thus, it is used as the connection topology of INOWFs, and the explicit connection topology constraints of INOWFs are defined, as shown in (16)–(22). Equations (16) and (17) describe the relationship between the connection topology variables of the collector and transmission systems of the new DSR topology, respectively. Equation (18) is an analytical connectivity constraint defined based on the network flow method to avoid topological islanding, where each network flow variable has no physical meaning [30]. And equation (19) is the OWF reliability constraint based on topological redundancy ω, where ω represents the redundancy degree of the OWF topology [31]. When the ω value increases, the number of submarine cable connections also increases, resulting in more paths for collecting and transmitting wind power. This reduces wind power losses caused by submarine cable outage, thereby improving the OWF's reliability, as shown in Fig. 2. Equation (20) is a constraint on the number of PCCs, offshore substations, and feeders connected to substations. Equation (21) is the investment limit of the total length of collector and transmission submarine cables; Equation (22) is the crossing-avoidance constraint of submarine cables. First, equation (23) is used to determine whether the two submarine cables ij and $i'j'$ cross, and if equation (23) is satisfied, equation (22) is used to avoid crossing. It should be noted that only the crossing-avoidance constraints of the cables in collector system need to be considered, whereas the crossing of the cables in transmission system can be avoided by planning the laying depth of submarine cables in actual projects.

$$\begin{cases}u_{ij}^c+u_{ji}^c\leqslant 1,\ u_{ij}^c\in\{0,1\},\ \forall i,j\in\Omega_{Bc}\\ \sum_{j\in\Omega_{Bc}}u_{ij}^c=1,\ \sum_{i\in\Omega_{Bc}}u_{ij}^c=1,\ \ \forall i,j\in\Omega_{wt}\\ \sum_{j\in\Omega_{Bc}}u_{sj}^c=\sum_{i\in\Omega_{Bc}}u_{is}^c,\ \ \forall s\in\Omega_s^{off}\end{cases} \tag{16}$$

$$u_{ij}^t+u_{ji}^t\leqslant 1,\ u_{ij}^t\in\{0,1\},\ \forall i,j\in\Omega_{Bt} \tag{17}$$

$$\begin{cases}q_i-q_{Li}=\sum_{j\in\Omega_{Bc/t}}q_{ij}\\ -\left(u_{ij}^{c/t}+u_{ji}^{c/t}\right)q_{\max}\leqslant q_{ij}\leqslant\left(u_{ij}^{c/t}+u_{ji}^{c/t}\right)q_{\max}\\ q_{ij}=-q_{ji}\\ q_{ii}=0\end{cases} \tag{18}$$

$$\begin{cases}\omega_{\min}\leqslant\omega\leqslant\omega_{\max}\\ \omega=\left(\sum_{i\in\Omega_{Bc}}\sum_{j\in\Omega_{Bc}}u_{ij}^c+\sum_{i\in\Omega_{Bt}}\sum_{j\in\Omega_{Bt}}u_{ij}^t\right)\Big/n_L\end{cases} \tag{19}$$

$$\begin{cases}N_{\min}^{PCC}\leqslant\sum_{n\in\Omega_{PCC}}z_n\leqslant N_{\max}^{PCC},\ z_n\in\{0,1\}\\ N_{SC,\min}\leqslant\sum_{s\in\Omega_s^{off}}z_s\leqslant N_{SC,\max},\ z_s\in\{0,1\}\\ z_sN_{Fc,\min}\leqslant\sum_{i\in\Omega_{Bc}}u_{is}^c+\sum_{j\in\Omega_{Bc}}u_{sj}^c\leqslant z_sN_{Fc,\max},\forall s\in\Omega_s^{off}\\ z_sN_{Ft,\min}\leqslant\sum_{i\in\Omega_{Bt}}u_{is}^t+\sum_{j\in\Omega_{Bt}}u_{sj}^t\leqslant z_sN_{Ft,\max},\\ \qquad\forall s\in\Omega_s^{off}\bigcup\Omega_s^{on}\end{cases} \tag{20}$$

$$\sum_{i\in\Omega_{Bc}}\sum_{j\in\Omega_{Bc}}u_{ij}^cL_{ij}\leqslant L_{inv.c},\ \sum_{i\in\Omega_{Bt}}\sum_{j\in\Omega_{Bt}}u_{ij}^tL_{ij}\leqslant L_{inv.t} \tag{21}$$

$$u_{ij}^{c}+u_{ji}^{c}+u_{i'j'}^{c}+u_{j'i'}^{c}\leqslant 1 \tag{22}$$

$$\begin{cases}\left[y_{i'}-f_{ij}(x_{i'})\right]\times\left[y_{j'}-f_{ij}(x_{j'})\right]<0\\ \left[y_{i}-f_{i'j'}(x_{i})\right]\times\left[y_{j}-f_{i'j'}(x_{j})\right]<0\end{cases} \tag{23}$$

where for q_i, if i is an onshore substation bus, $q_i=q_s$, otherwise $q_i=0$; for $q_{\mathrm{L}i}$, if i is a WT bus, $q_{\mathrm{L}i}=1$, otherwise $q_{\mathrm{L}i}=0$; $q_{\max}$ is a given positive integer, limiting the number of WTs connected by each ring structure in the collector system to a maximum of $2q_{\max}$; For z_s, if the candidate onshore substation s is connected to PCC n, $z_s=z_n$; $f_{ij}(\cdot)$ is the linear function representing the straight line passing through buses i and j; and $f_{i'j'}(\cdot)$ has a similar meaning.

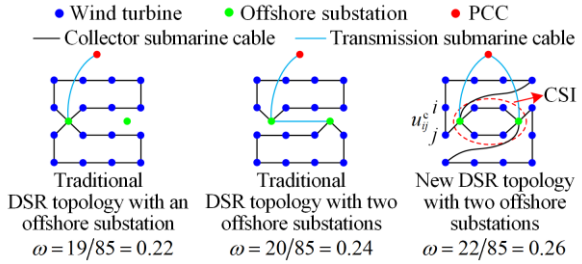

Fig. 2. Redundancy of the traditional and new DSR topologies.

2) Type Selection Constraints of Electrical Devices

The collector and transmission submarine cables and transformers need to select one of types, as:

$$\begin{cases}u_{ij}^{c}=\sum_{k\in\Omega_{cc}}u_{kij}^{c},u_{kij}^{c}\in\{0,1\}\\ u_{ij}^{t}=\sum_{h\in\Omega_{ct}}u_{hij}^{t},u_{hij}^{t}\in\{0,1\}\\ z_s=\sum_{p\in\Omega_{TR}}z_{p,s},z_{p,s}\in\{0,1\}\end{cases} \tag{24}$$

3) Power Flow Constraints of INOWFs

The injected power from each OWF to the OTN at the PCC is subject to certain limitations, as shown in (25), which avoids the low utilization rate of an OWF's transmission system caused by the low injected power at the PCC.

$$\lambda P_{\Sigma nz_n}\leqslant P_{ni}^{\mathrm{PCC}}\leqslant P_{\Sigma nz_n} \tag{25}$$

For the collector system, based on the approximate linear AC power flow equations in [29], the AC power flow constraints considering the connection topology changes are shown as:

$$\begin{cases}P_i^{c}=\sum_{j\in i}P_{ij}^{c},\ Q_i^{c}=\sum_{j\in i}Q_{ij}^{c}\\ -M\left[1-\left(u_{ij}^{c}+u_{ji}^{c}\right)\right]\leqslant P_{ij}^{c}-\left[\sum_{k\in\Omega_{cc}}\left(u_{kij}^{c}+u_{kji}^{c}\right)g_{ck}\right]\times\\ \quad L_{ij}\left(U_i^{c}-U_j^{c}\right)+\left[\sum_{k\in\Omega_{cc}}\left(u_{kij}^{c}+u_{kji}^{c}\right)b_{ck}\right]L_{ij}\left(\theta_i^{c}-\theta_j^{c}\right)\leqslant\\ \quad M\left[1-\left(u_{ij}^{c}+u_{ji}^{c}\right)\right]\\ -M\left[1-\left(u_{ij}^{c}+u_{ji}^{c}\right)\right]\leqslant Q_{ij}^{c}+\left[\sum_{k\in\Omega_{cc}}\left(u_{kij}^{c}+u_{kji}^{c}\right)b_{ck}\right]\times\\ \quad L_{ij}\left(U_i^{c}-U_j^{c}\right)+\left[\sum_{k\in\Omega_{cc}}\left(u_{kij}^{c}+u_{kji}^{c}\right)g_{ck}\right]L_{ij}\left(\theta_i^{c}-\theta_j^{c}\right)\leqslant\\ \quad M\left[1-\left(u_{ij}^{c}+u_{ji}^{c}\right)\right]\end{cases} \tag{26}$$

where if bus i is connected to WT w, $P_i^{c}=P_{wi}$ and $Q_i^{c}=Q_{wi}$; if bus i is connected to offshore substation s, $P_i^{c}=-P_{si}^{ac}$ and $Q_i^{c}=-Q_{si}^{ac}$; and $j\in i$ represents all buses j that might be connected to bus i.

For the transmission system, if the VSC-MTDC transmission mode is adopted, the DC power flow constraints considering connection topology changes are shown in (27). If the AC transmission mode is adopted, the AC power flow constraints considering connection topology changes are similar to (26).

$$\begin{cases}P_i^{t}=\sum_{j\in i}P_{ij}^{t}\\ -M\left[1-\left(u_{ij}^{t}+u_{ji}^{t}\right)\right]\leqslant P_{ij}^{t}-\left[\sum_{h\in\Omega_{ct}}\left(u_{hij}^{t}+u_{hji}^{t}\right)g_{th}\right]\times\\ \quad L_{ij}\left(U_i^{t}-U_j^{t}\right)\leqslant M\left[1-\left(u_{ij}^{t}+u_{ji}^{t}\right)\right]\end{cases} \tag{27}$$

where if bus i is connected to an offshore or onshore substation s, then $P_i^{t}=P_{si}^{dc}$.

For the VSC-MTDC transmission mode, the steady-state equations of the VSC stations are given in (28)–(31) [32]. Equations (28) and (29) are the transmission power limitations on the AC side, while equations (30) and (31) are the relationships of active power and voltage magnitude between the AC and DC sides, respectively.

$$z_sP_{s,\min}^{ac}\leqslant P_{si}^{ac}\leqslant z_sP_{s,\max}^{ac} \tag{28}$$

$$z_sQ_{s,\min}^{ac}\leqslant Q_{si}^{ac}\leqslant z_sQ_{s,\max}^{ac} \tag{29}$$

$$P_{si}^{ac}=P_{si}^{dc} \tag{30}$$

$$U_s^{ac}=(\mu K_{\mathrm{A}}/\sqrt{2})U_s^{dc} \tag{31}$$

where if onshore converter station s is connected to PCC n, $P_{si}^{ac}=P_{ni}^{\mathrm{PCC}}$, and $Q_{si}^{ac}=Q_{ni}^{\mathrm{PCC}}$; μ is the DC voltage utilization rate, which is set to $\sqrt{3}/2$; while K_{A} is the modulation ratio, which is set to $[0,1]$. The equivalent impedance of the converter can be incorporated into the line parameters.

Equation (31) can be simplified to:

$$0\leqslant U_s^{ac}\leqslant(\sqrt{6}/4)U_s^{dc} \tag{32}$$

In addition, the simplified forms of the active and reactive output constraints of offshore WTs are as (33), while the simplified forms of the bus voltage security constraints and the phase angle difference constraints are given as (34) and (35), respectively. Their specific models are described in detail in [27]. Specifically, $P_{wi\min}$ in (33) is determined by the minimum technical power output of offshore WTs, and $P_{wi\max}$ in (33) is obtained based on the wind speed of OWFs and the wake effect model, as detailed in [32].

$$\boldsymbol{h}_1\left(P_{wi},Q_{wi},P_{wi\min},P_{wi\max},\varphi_{w\min},\varphi_{w\max}\right)\leqslant 0 \tag{33}$$

$$\boldsymbol{h}_2\left(U_i^{c},U_i^{t},U_{i\min}^{c},U_{i\min}^{t},U_{i\max}^{c},U_{i\max}^{t}\right)\leqslant 0 \tag{34}$$

$$\boldsymbol{h}_3\left(u_{ij}^{c},\theta_{ij}^{c},\theta_{ij\min}^{c},\theta_{ij\max}^{c}\right)\leqslant 0 \tag{35}$$

If the AC transmission mode is adopted, the phase angle constraints in the transmission system are similar to (35).

4) Capacity Constraints of Submarine Cables and Transformers

The capacity planning of submarine cables and transformers needs to ensure a certain margin to handle the line outage in OWFs, and the corresponding capacity constraints are as follows:

$$\begin{aligned}-\gamma\sum_{k\in\Omega_{cc}}\left(I_{n,k}U_{\mathrm{N}}^{c}\right)\left(u_{kij}^{c}+u_{kji}^{c}\right)&\leqslant P_{ij}^{c}/\cos\varphi_{ij}\\ &\leqslant\gamma\sum_{k\in\Omega_{cc}}\left(I_{n,k}U_{\mathrm{N}}^{c}\right)\left(u_{kij}^{c}+u_{kji}^{c}\right)\end{aligned} \tag{36}$$

$$-\gamma\sum_{h\in\Omega_{\mathrm{ct}}}P_{\mathrm{n},h}\left(u_{hij}^{\mathrm{t}}+u_{hji}^{\mathrm{t}}\right)\leqslant P_{ij}^{\mathrm{t}}\leqslant\gamma\sum_{h\in\Omega_{\mathrm{ct}}}P_{\mathrm{n},h}\left(u_{hij}^{\mathrm{t}}+u_{hji}^{\mathrm{t}}\right) \tag{37}$$

$$-\gamma\sum_{p\in\Omega_{\mathrm{TR}}}2S_{\mathrm{TN},p}z_{p,s}\leqslant P_{si}^{\mathrm{ac}}/\cos\varphi_s\leqslant\gamma\sum_{p\in\Omega_{\mathrm{TR}}}2S_{\mathrm{TN},p}z_{p,s} \tag{38}$$

If the AC transmission mode is adopted, the capacity constraints of submarine cables in the transmission system are similar to (36).

In the proposed CP model of multiple INOWFs and OTE, the objective function is given by (1)–(3), and the constraints include (4)–(22), (24)–(30) and (32)–(38). The proposed CP model is suitable for INOWFs with the new DSR topology but can also be applied to INOWF planning with other topologies by modifying the connection topology constraints (16)–(22). However, since the proposed CP model has numerous binary variables and equations (3), (13), (26), and (27) include many nonlinear terms, the proposed model is a large-scale mixed integer nonlinear programming (MINLP) model, which is difficult to solve efficiently and accurately. Therefore, the proposed CP model needs to be further processed before it can be solved.

IV. Solution Methodology

Since the proposed CP model is a large-scale MINLP model, efficient solving techniques such as convexification, reducing the binary variables, contracting the feasible region and using the DCP algorithm are adopted to solve the model and obtain the optimal CP scheme.

A. Convexification of the CP Model

In the proposed CP model, there are two nonlinear terms, namely, $\tau\kappa^2$ in the objective function (3) and $\tau\kappa$ in the constraints (13), (26), and (27), where τ is a binary variable and κ is a continuous variable. Since $\tau\kappa^2=(\tau\kappa)^2$, only term $\tau\kappa$ needs to be convex. By introducing an intermediate variable $\delta=\tau\kappa$, replacing the nonlinear term $\tau\kappa$ with δ and applying the big M-method to incorporate the convex constraints (39) into the model, the objective function is transformed into a quadratic function related to δ^2, while all constraints remain linear with respect to δ. This means that the original non-convex model is transformed into a mixed integer quadratic programming (MIQP) model.

$$\begin{cases}-M\tau\leqslant\delta\leqslant M\tau\\ -M\left(1-\tau\right)\leqslant\delta-\kappa\leqslant M\left(1-\tau\right)\end{cases} \tag{39}$$

B. Reduction of Binary Variables

Obviously, a shorter connection distance between buses for submarine cables results in lower investment cost. Therefore, in order to reduce the complexity of solving the proposed CP model, each bus in the collector system is only considered for submarine cable connections with buses within a certain distance range. Beyond this range, submarine cable connections are deemed infeasible. In other words, a topological connection is considered only if the distance between buses i and j satisfies the condition of $\sqrt{(x_i-x_j)^2+(y_i-y_j)^2}\leqslant r_{\max}$, where $r_{\max}$ is the maximum allowable distance for a potential connection.

In addition, due to the geographical location and regulatory restrictions in actual power systems, it is unrealistic to consider all possible situations to build new transmission corridors in the OTN. Therefore, a set of candidate newly-built transmission corridors is determined before the planning process by selecting the transmission corridors near the PCCs of OWFs and in the areas with a high load demand. The situations where there is no connection between buses and a new transmission corridor is required are considered only from this set.

C. Parallel Random Search Method for Feasible Region Contraction

There are many binary variables related to the INOWF planning, which can lead to slow convergence when solving the proposed CP model due to the vast number of possible combinations. To mitigate this, a PRS method is proposed to obtain the set of feasible connection topology schemes for each INOWF, thereby constraining the feasible region and improving the efficiency of solving the CP model. Taking the connection topology constraints (16)–(22) as the constraints and setting the objective function to be an arbitrary constant value, a random search model for feasible connection topology schemes of an INOWF is established, shown as:

$$\min\sigma_{\mathrm{c}},\ \text{s.t. (16)}-\text{(22)} \tag{40}$$

where σ_{c} is an arbitrary constant.

Each time when model (40) is solved, a feasible connection topology scheme of the INOWF is obtained. In the subsequent iterations of the random search model (40), an additional constraint (41) is added to prevent the repetition of the previously obtained connection topology schemes. After multiple iterations, if no feasible solution is found or the predefined maximum searching number is reached, the set Ω_{TC} of feasible connection topology schemes for each INOWF is obtained.

$$\sum_{\xi_k^{(b-1)}=0}(1-\xi_k)+\sum_{\xi_k^{(b-1)}=1}\xi_k\leqslant N_\xi-1 \tag{41}$$

where $\xi_k\in\left\{u_{ij}^{\mathrm{c}},u_{ij}^{\mathrm{t}},z_n,z_s\right\}$; $\xi_k^{(b-1)}$ is the value of binary variable ξ_k after the last search; and N_ξ is the total number of ξ_k.

To search the feasible connection topology schemes to form the set Ω_{TC} more efficiently, the topological redundancy range $[\omega_{\min},\omega_{\max}]$ in (19) can be divided into N_ω sub-intervals $[\omega_i,\omega_{i+1}]$, and the range of the number of PCCs $[N_{\min}^{\mathrm{PCC}},N_{\max}^{\mathrm{PCC}}]$ in (20) can be divided into N_{PCC} sub-intervals $[N_i,N_{i+1}]$, as shown in (42). In $N_\omega\times N_{\mathrm{PCC}}$ sub-interval combination scenarios of $[\omega_i,\omega_{i+1}]$ and $[N_i,N_{i+1}]$, the maximum searching number $N_{\max}^{\mathrm{cs}}$ for each combination scenario is given, and the set Ω_{TC} can be obtained after searching $N_\omega\times N_{\mathrm{PCC}}\times N_{\max}^{\mathrm{cs}}$ feasible connection topology schemes from different directions. Moreover, by using parallel computing to search for feasible connection topology

schemes related to each scenario from $N_\omega \times N_{\mathrm{PCC}}$ combination scenarios, the computational efficiency can be improved. By using Ω_{TC}, the feasible region of the proposed CP model can be contracted after replacing the original connection topology constraints (16)–(22) with (43). In the subsequent solution of the proposed CP model, the optimal connection topology scheme for each INOWF is searched from the set Ω_{TC}.

$$\begin{cases} \omega_i = \omega_{\min} + i\left(\omega_{\max} - \omega_{\min}\right)/N_\omega,\ i = 0,1,\cdots,N_\omega \\ N_i = N_{\min}^{\mathrm{PCC}} + i\left(N_{\max}^{\mathrm{PCC}} - N_{\min}^{\mathrm{PCC}}\right)/N_{\mathrm{PCC}},\ i = 0,1,\cdots,N_{\mathrm{PCC}} \end{cases} \tag{42}$$

$$\begin{cases} \sum_{u\in\Omega_{\mathrm{TC}}} H_u = 1,\ H_u \in \{0,1\} \\ u_{ij}^{\mathrm{c}} = \sum_{u\in\Omega_{\mathrm{TC}}} H_u u_{iju}^{\mathrm{c}},\ u_{ij}^{\mathrm{t}} = \sum_{u\in\Omega_{\mathrm{TC}}} H_u u_{iju}^{\mathrm{t}} \\ z_s = \sum_{u\in\Omega_{\mathrm{TC}}} H_u z_{s,u},\ z_n = \sum_{u\in\Omega_{\mathrm{TC}}} H_u z_{n,u} \end{cases} \tag{43}$$

where H_u is a binary variable indicating whether to select the uth connection topology scheme; while u_{iju}^{c}, u_{iju}^{t}, $z_{s,u}$ and $z_{n,u}$ are the values of connection topology variables in the uth connection topology scheme.

Therefore, after the convexification, reduction of binary variables and feasible region contraction, the original large-scale MINLP model for CP is transformed into a more tractable and small scale MIQP model:

$$\begin{aligned} &\min\ f_{\mathrm{TE}} + \textstyle\sum_{m\in\Omega_{\mathrm{F}}} f_{\mathrm{OWF},m}, \\ &\text{s.t. } (2)-(15),(24)-(30),(32)-(39),(43) \end{aligned} \tag{44}$$

D. Decomposition and Coordination Planning Algorithm

When the proposed CP method is applied to actual large-scale power systems with OWFs, centralized solution becomes very complex due to the large-scale optimization model. Therefore, by dividing the entire system into the OTN and multiple OWFs, a DCP algorithm is proposed to solve the proposed CP model (44) through alternating iterations and to obtain the optimal CP scheme efficiently.

According to the boundary coupling variables P_{ni}^{PCC}, Q_{ni}^{PCC}, U_i and θ_i at PCCs, the proposed CP model (44) of multiple INOWFs and OTE is decomposed into the planning sub-model of OTE that is a mixed integer linear programming model and the planning sub-model of each INOWF that is a MIQP model, as shown in Fig. 3. These two sub-models can be efficiently solved by using the mature commercial solver GUROBI directly, and they are shown as (45) and (46) in the rth iteration.

$$\begin{aligned} &\min_{\boldsymbol{x}_1, U_i, \theta_i}\ f_{\mathrm{TE}}\left(\boldsymbol{x}_1, P_{ni}^{\mathrm{PCC}(r-1)}, Q_{ni}^{\mathrm{PCC}(r-1)}, U_i, \theta_i\right), \\ &\text{s.t. } (2),(4),(8)-(15),(39) \end{aligned} \tag{45}$$

$$\begin{aligned} &\min_{\boldsymbol{x}_2, P_{ni}^{\mathrm{PCC}}, Q_{ni}^{\mathrm{PCC}}}\ f_{\mathrm{OWF}}\left(\boldsymbol{x}_2, P_{ni}^{\mathrm{PCC}}, Q_{ni}^{\mathrm{PCC}}, U_i^{(r-1)}, \theta_i^{(r-1)}\right), \\ &\text{s.t. } (3),(5)-(7),(24)-(30),(32)-(39),(43) \end{aligned} \tag{46}$$

where $\boldsymbol{x}_1$ and $\boldsymbol{x}_2$ are the decision variables of the OTE planning and INOWF planning, respectively; $P_{ni}^{\mathrm{PCC}(r-1)}$ and $Q_{ni}^{\mathrm{PCC}(r-1)}$ are the results obtained by solving (46) in the x_1 $(r-1)$th iteration; while $U_i^{(r-1)}$ and $\theta_i^{(r-1)}$ are the results obtained by solving (45) in the $(r-1)$th iteration.

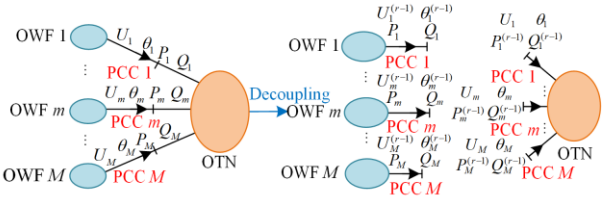

Fig. 3. Decoupling by the bus tearing method.

In each iteration, $P_{ni}^{\mathrm{PCC}(r-1)}$ and $Q_{ni}^{\mathrm{PCC}(r-1)}$ which are transferred from sub-model (46) are used first to solve sub-model (45), while $U_i^{(r)}$ and $\theta_i^{(r)}$ at PCCs for each INOWF are then obtained and transferred to sub-model (46). Next, according to the independence of the planning of each INOWF, $U_i^{(r)}$ and $\theta_i^{(r)}$ are used to solve each sub-model (46) in parallel, while $P_{ni}^{\mathrm{PCC}(r)}$ and $Q_{ni}^{\mathrm{PCC}(r)}$ at PCCs for each INOWF are obtained and transferred to sub-model (45). Finally, sub-models (45) and (46) are solved multiple times through alternating iterations until convergence criterion (47) is satisfied, and the optimal CP scheme of multiple INOWFs and OTE is obtained. The flowchart of the proposed DCP algorithm is shown in Fig. 4.

$$\Delta = \left\| \boldsymbol{\chi}^{(r)} - \boldsymbol{\chi}^{(r-1)} \right\|_2 \leqslant \varepsilon \tag{47}$$

where $\boldsymbol{\chi} = \left(P_{ni}^{\mathrm{PCC}}, Q_{ni}^{\mathrm{PCC}}, U_i, \theta_i\right)$, and ε is the convergence threshold.

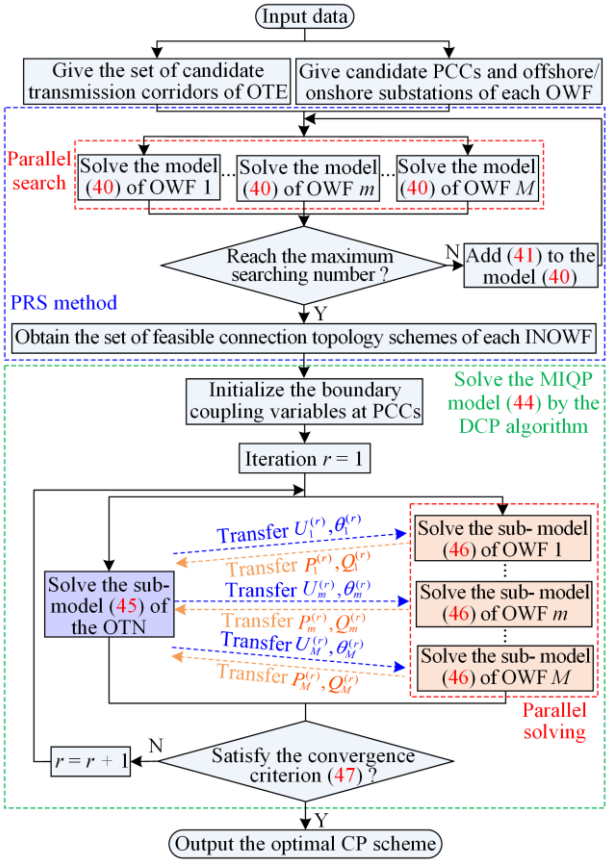

Fig. 4. Flowchart of the proposed DCP algorithm.

V. Case Studies

Case studies are executed on the modified IEEE 39-bus system with two OWFs to be planned and an actual provincial power system with six OWFs to be planned. For the OTE, the maximum number of lines in a transmission corridor $N_{ij\max}$ is 3. Considering the increase in loads, the load power demand is set as 1.3 times the initial load power. For the INOWFs, the rated voltage of the AC collector system is 35 kV. For the AC transmission mode, the rated voltage is 220 kV, while for the VSC-MTDC transmission mode, the rated voltage is ± 320 kV. The expansion cost of transmission corridors and the cost parameters of AC/DC submarine cables can be found in [11], [21], [28]. The types of AC/DC submarine cables and transformers are presented in Tables AI–AIII in Appendix A. The maximum distance $r_{\max}$ is 3.8 km, and the value of M in the big M-method is 50 000. In the PRS method, $N_{\omega}=5$, $N_{\mathrm{PCC}}=2$, and $N_{\max}^{\mathrm{cs}}=300$. The convergence threshold $\varepsilon=10^{-5}$. The computing platforms are GAMS 41.5 and Matlab 2020b. The parallel computation is executed using a blade cluster composed of 24 HPE BL460C GEN10 computing blades, where each computing blade is composed of two 2.30-GHz Intel Gen10 Xeon-G 5118 (12 cores) processors and 128 GB of RAM.

A. Modified IEEE 39-bus System with Two OWFs

1) System Parameters

The modified IEEE 39-bus system includes an existing OWF, an existing photovoltaic (PV) station, and two OWFs to be planned, as displayed in Fig. 5. The rated capacities of the existing OWF and PV station are 400 MW and 500 MW, connected to buses 18 and 14 in the OTN, respectively. The number of WTs in the OWF1 to be planned is 36, and the rated power of each WT is 8 MW. OWF1 adopts AC collector and AC transmission mode, and has three candidate PCCs (buses 8, 9, 39 in the OTN). The number of WTs in the OWF2 to be planned is 78, and the rated power of each WT is 6.45 MW. OWF2 adopts AC collector and VSC-MTDC transmission mode, and has three candidate PCCs (buses 4, 5, 6 in the OTN).

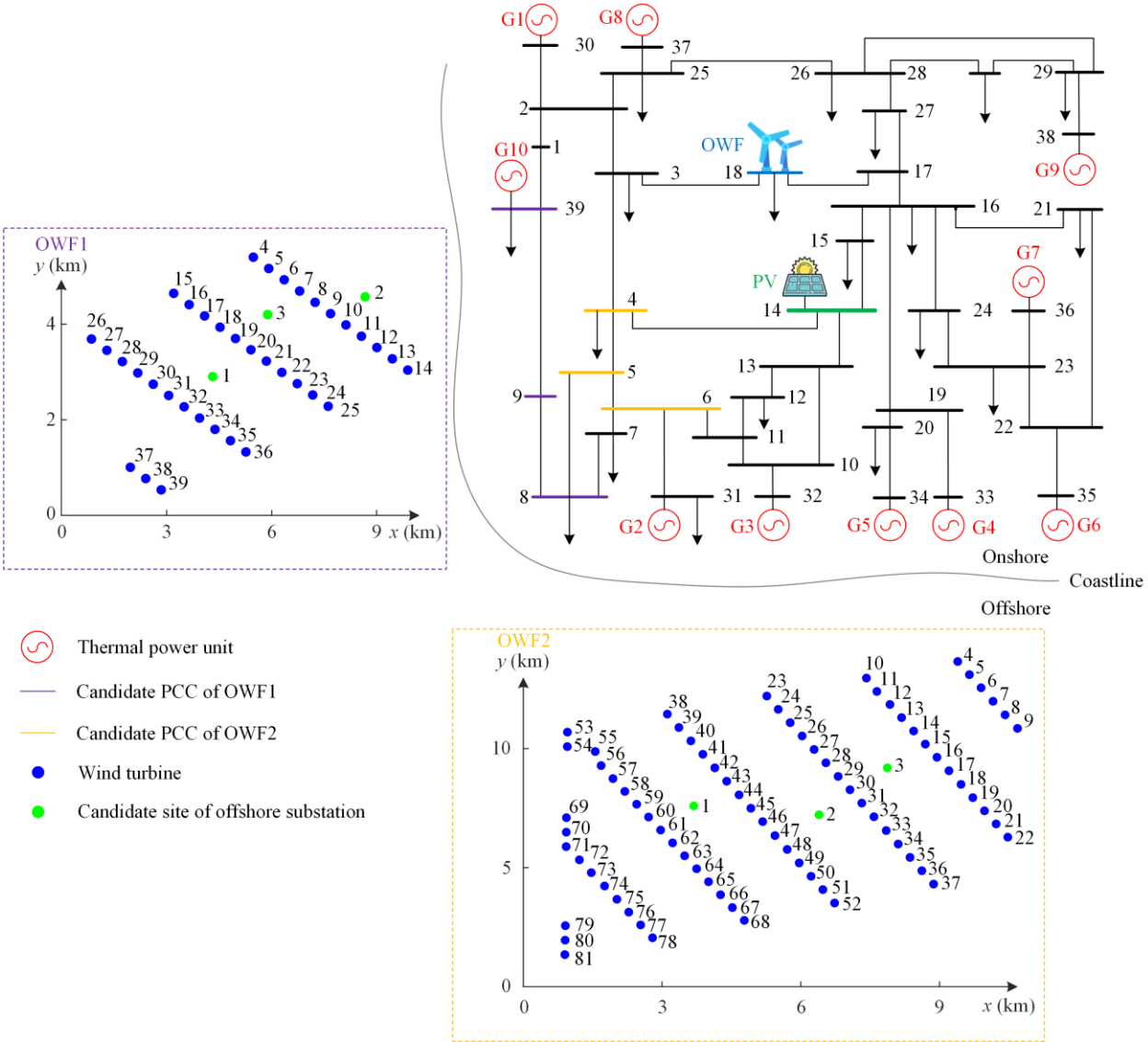

Fig. 5. Modified IEEE 39-bus system with two OWFs to be planned.

2) Analysis of Optimal Planning Results

The proposed CP model is solved by using the DCP algorithm, and the optimal CP results and scheme (denoted by S1) are obtained as displayed in Table I and Fig. 6(a). It can be seen that in order to accommodate wind power and meet the increasing load demands, the proposed CP model prioritizes the expansion of transmission corridors that are shorter in distance and effectively alleviate line congestion in the OTN, ultimately aiming to minimizing overall planning cost. Therefore, the obtained optimal CP scheme plans a total of four newly-built transmission lines, namely lines 2–3, 6–11, 10–11, and 23–24. For OWF1 with a smaller total installed capacity, two offshore substations, one onshore substation and one PCC are planned, while for OWF2 with a larger total installed capacity, two offshore substations, two onshore substations and two PCCs are planned. At the same time, the wind curtailment costs of two OWFs are zero. It is proved that the proposed CP model can optimize and select the number of offshore/onshore substations and PCCs to accommodate wind power at low economic costs. Although the total length of AC collector submarine cables planned for OWF1 and OWF2 is long, however, Type 1 submarine cables with a smaller capacity and a lower cost account for the highest proportion. This is because the topology optimization of INOWFs considers the new DSR topology with CSI, which provides multiple paths for the collection and transmission of the WT power and balances the distribution of the OWF power flow.

TABLE I
OPTIMAL PLANNING RESULTS OF DIFFERENT SCENARIOS

Network	Item		S1	S2
OTN	Annual investment cost (10^3¥)		996.6	1610.5
	C_{op} (10^3¥)		276 116.5	276 317.6
	f_{TE} (10^3¥)		277 113.1	277 928.1
	Number of newly-built transmission lines		4	7
OWF1	C_{in} (10^3¥)		246 155.4	239 214.8
	C_{lo} (10^3¥)		15 325.6	24 631.7
	C_{wc} (10^3¥)		0	0
	f_{OWF} (10^3¥)		261 481.0	263 846.5
	Number of offshore/onshore substations		2/1	2/1
	Number of PCCs		1	1
	Total length of AC collector submarine cables (km)	Type 1	41.49	15.60
		Type 2	14.82	6.45
		Type 3	0.96	6.38
		Sum	57.27	28.43
	Total length of AC transmission submarine cables (km)	Type 1	0	4.26
		Type 2	4.26	12.91
		Type 3	13.60	0
		Sum	17.86	17.17
	Single transformer capacity of offshore substations (MVA)		{120, 120}	{120, 120}
	EENS (MWh)		90 663	163 520
OWF2	C_{in} (10^3¥)		540 788.7	633 375.6
	C_{lo} (10^3¥)		52 782.8	75 398.0
	C_{wc} (10^3¥)		0	416 798.1
	f_{OWF} (10^3¥)		593 571.5	1125 571.7
	Number of offshore/onshore substations		2/2	2/2
	Number of PCCs		2	2
	Total length of AC collector submarine cables (km)	Type 1	72.77	61.43
		Type 2	24.45	20.12
		Type 3	32.14	16.83
		Sum	129.36	98.38
	Total length of DC transmission submarine cables (km)	Type 1	76.42	81.57
		Type 2	0	0
		Sum	76.42	81.57
	Single transformer capacity of offshore substations (MVA)		{120, 250}	{250, 250}
	EENS (MWh)		103 759	166 609

3) Comparison of Optimal Planning Results Considering Different INOWF Topologies

To analyze the impact of different INOWF topologies on the optimal CP scheme, another scenario is constructed and denoted by S2, where the connection topology constraint (16) is modified according to [6] to consider the optimization of the radial topology in the planning. The optimal planning results and schemes of S1–S2 are shown in Table I and Fig. 6. The results of the expected energy not supplied (EENS) reflecting the degree of reliability in Table I can be calculated according to [8]. For the OTE planning, because the grid-connected power at PCCs of S2 is relatively large, severe onshore transmission line congestion arises. Therefore, S2 needs to expand more new transmission lines, and its investment cost of the OTN increases by 61.6% compared with S1. For the planning of OWF1 and OWF2, compared with S2, S1 optimizes the new DSR topology on the basis of ensuring minimal wind curtailment, while the CSI balances power flow and maintains the high reliability of the ring topology. Thus, the EENSs of OWF1 and OWF2 in S1 are 44.6% and 37.7% lower than S2, respectively. In addition, the annual equivalent power loss costs of OWF1 and OWF2 in S1 are 37.8% and 30.0% lower than S2, respectively. Comparison of the optimal CP results of S1 and S2 indicates that the proposed CP model can simultaneously obtain the most economical expansion planning scheme of OTN and the optimal planning schemes of multiple INOWFs that consider the economics and reliability. Therefore, compared with the radial topology, the new DSR topology applied in INOWFs can share capacity between offshore substations to reduce power losses and improve reliability, which significantly helps to accommodate offshore wind power.

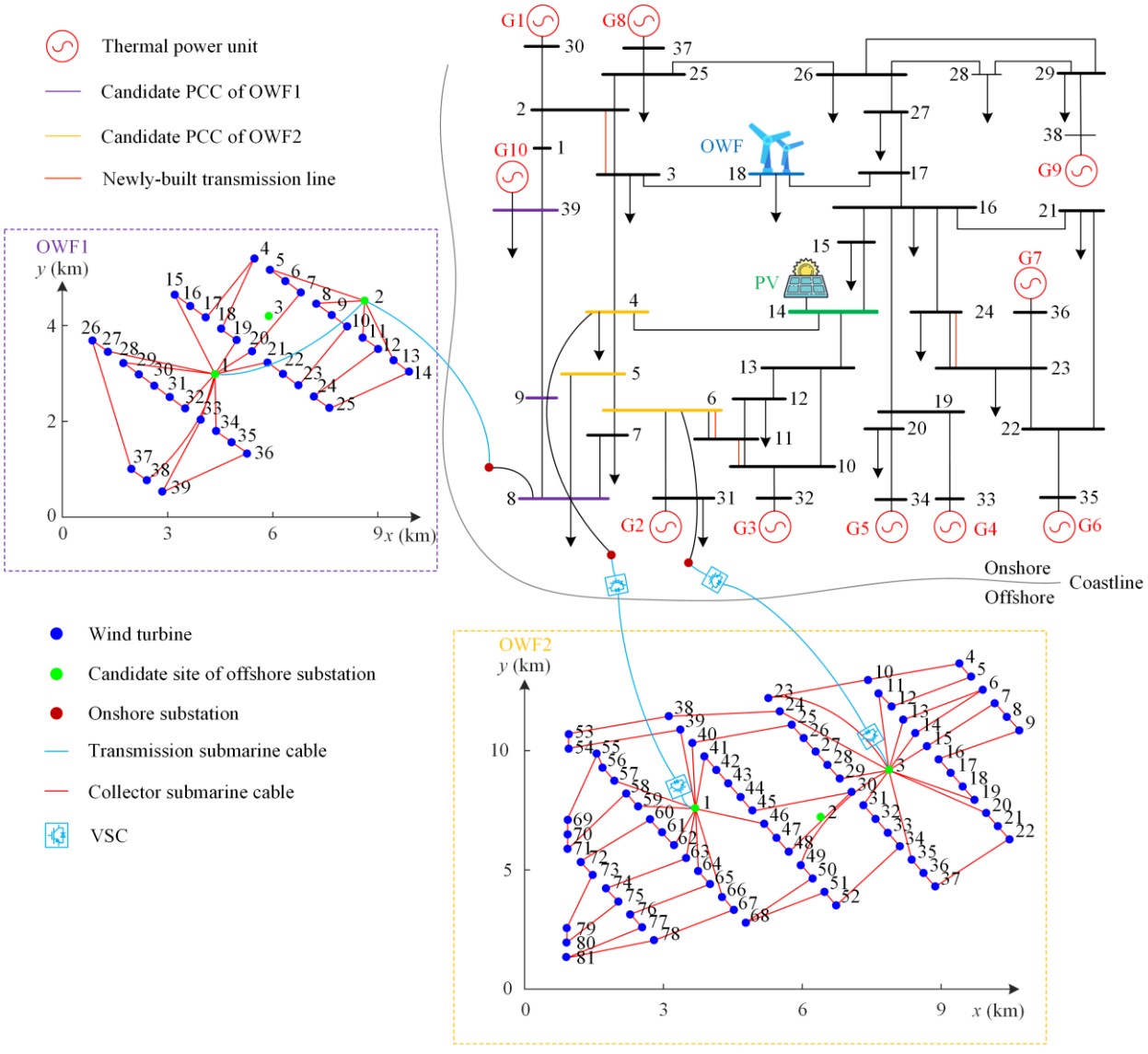

(a)

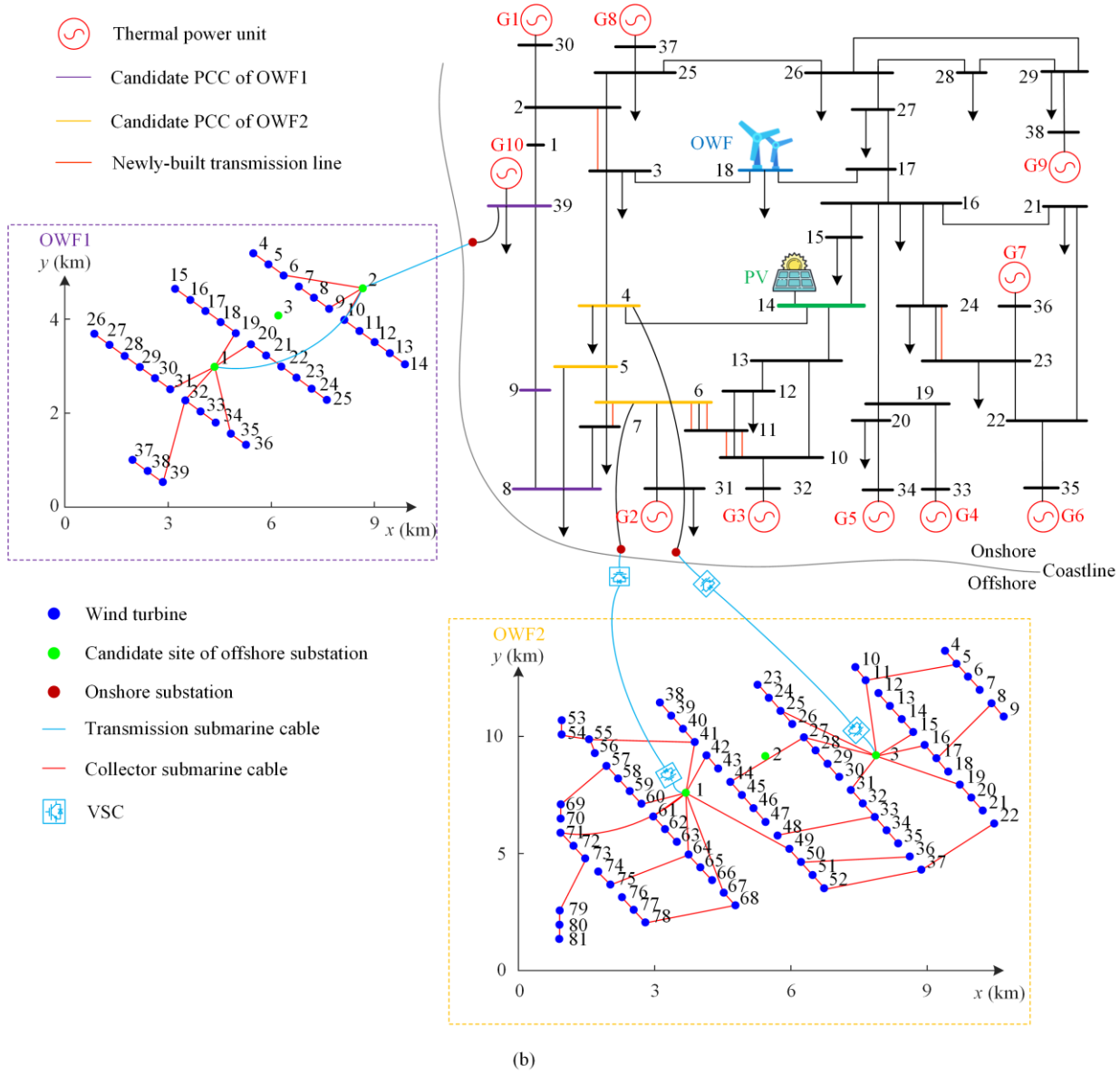

(b)

Fig. 6. Optimal planning schemes of different scenarios. (a) S1. (B) S2.

4) Effectiveness Analysis of the PRS Method

To demonstrate the effectiveness of the proposed PRS method for feasible connection topology schemes of INOWFs, first, the connection topology constraints (16)–(22) are directly added to the CP model and the model is solved by the DCP algorithm without PRS method. Due to large numbers of binary variables, the DCP algorithm without PRS method has difficulty in converging and cannot obtain the optimal CP scheme. Then, given $N_{\omega}=5$ and $N_{\mathrm{PCC}}=2$, different total numbers of feasible connection topology schemes for each INOWF are obtained through the parallel search by changing the parameter $N_{\max}^{\mathrm{cs}}$. On this basis, the proposed DCP algorithm is used to solve the proposed CP model, and the corresponding parallel search time and annual equivalent OWF planning cost are shown in Fig. 7. As the searching number increases, the connection topology scheme with a lower annual equivalent planning cost is found, and better planning result is achieved. Obviously, the parallel search time also increases. However, when the total number of feasible connection topology schemes reaches 3000, the parallel search time is 3302.6 s. At this point, increasing the searching number has minimal impact on the annual equivalent planning cost and only results in wasted time. Therefore, after applying the PRS method to identify a sufficient number of feasible connection topology schemes of an INOWF, the optimal scheme can be included. Moreover, these results show that setting the maximum searching number $N_{\max}^{\mathrm{cs}}=300$ for each parallel scenario is appropriate and effective for contracting the feasible region and improving the search efficiency.

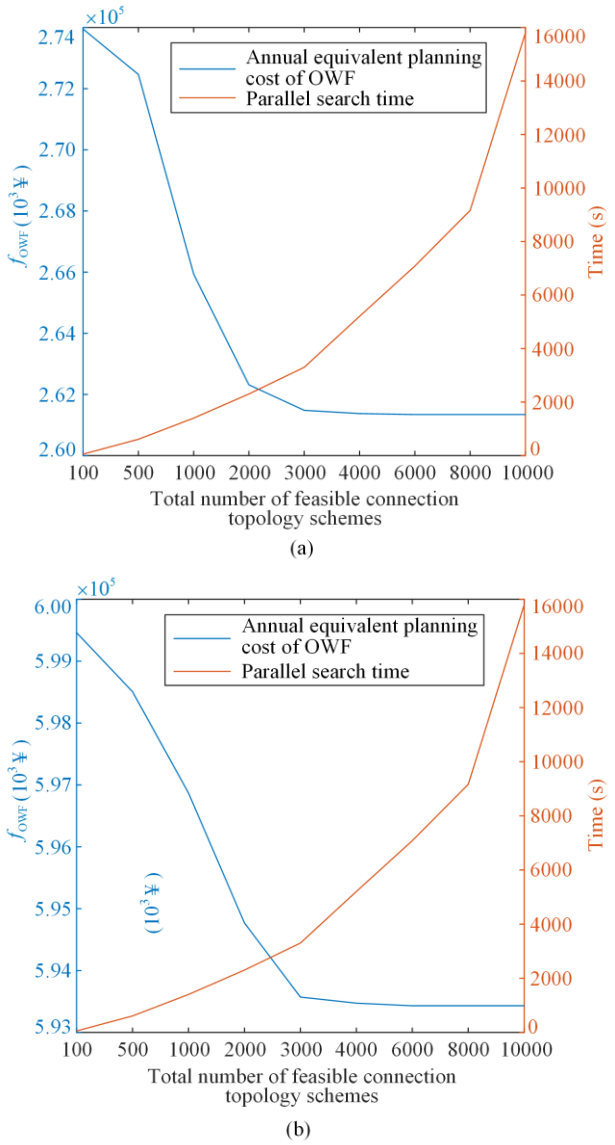

Fig. 7. Annual equivalent planning cost and parallel search time for a different number of connection topology schemes. (a) OWF1. (b) OWF2.

5) Comparison of Different Optimization Algorithms

To analyze the performance of the proposed DCP algorithm with PRS method, comparison with other three solution algorithms is conducted. For the algorithm used in [21]−[26], an OWF is only regarded as a variable power source injected into the PCC limited by its total installed capacity, and the PCC location is also given in advance. For the separated planning algorithm with PRS method, the planning of each INOWF is executed first, and then the OTE planning is executed based on the previous INOWF planning results. For the centralized planning algorithm with PRS method, the optimal CP scheme is obtained by centrally solving the proposed CP model. The optimal planning results of the four algorithms are presented in Table II. The sets Ω_{TC} of the PRS method for the last three algorithms are the same, and the parallel search time is 3302.6 s. The algorithm in [21]−[26] executes the OTE planning based on the predetermined OWF capacities and PCC locations, while ignoring the impact of INOWFs on the OTN and the INOWFs' optimization space. Thus, more new transmission lines are required to be expanded, resulting in the highest OTE planning cost. Moreover, this algorithm cannot obtain the optimal INOWF planning scheme. Although the CPU time consumed by the separated planning algorithm is the shortest among the last three algorithms, it does not consider the impact of INOWF planning on the power flow distribution and the line congestion of the OTE planning, and the two sub-problems are solved separately. Therefore, the separated planning algorithm cannot guarantee the lowest overall planning cost and lacks optimality. Compared with the centralized planning algorithm, the proposed DCP algorithm with PRS method can not only obtain a very close optimal planning scheme, but also converge after only three iterations, significantly reducing the consumed CPU time and improving the solution efficiency. The comparative results of the four algorithms show that the proposed DCP algorithm with PRS method can obtain the optimal CP scheme for multiple INOWFs and OTE, and achieve high solution efficiency.

TABLE II
OPTIMAL PLANNING RESULTS OF DIFFERENT ALGORITHMS

Algorithm	f_{TE} (10^3¥)	f_{OWF} of OWF1 (10^3¥)	f_{OWF} of OWF2 (10^3¥)	Total planning cost (10^3¥)	CPU time (s)
Algorithm in [21]−[26]	277 296.4				31.5
Separated planning with PRS	277 270.7	265 781.6	595 209.3	1 138 261.6	141.7
Centralized planning with PRS	277 112.8	261 480.7	593 571.3	1 132 164.8	823.2
DCP with PRS	277 113.1	261 481.0	593 571.5	1 132 165.6	399.4

B. Actual Provincial Power System with Six OWFs

1) System Parameters

The OTN of the actual provincial power system includes 2752 buses and 3003 branches, and is integrated with 178 thermal power units, 9 nuclear power units, 10 hydroelectric units, 4 pumped-storage hydro (PSH) stations, and 3 PV stations. Six OWFs are planned to be integrated into the power system. The topology of the 500 kV main network of the system and the relative locations of the six OWFs are shown in Fig. 8. The parameters of the PSH and PV stations are given in Table AIV of Appendix A, while the parameters of six OWFs are given in Table III.

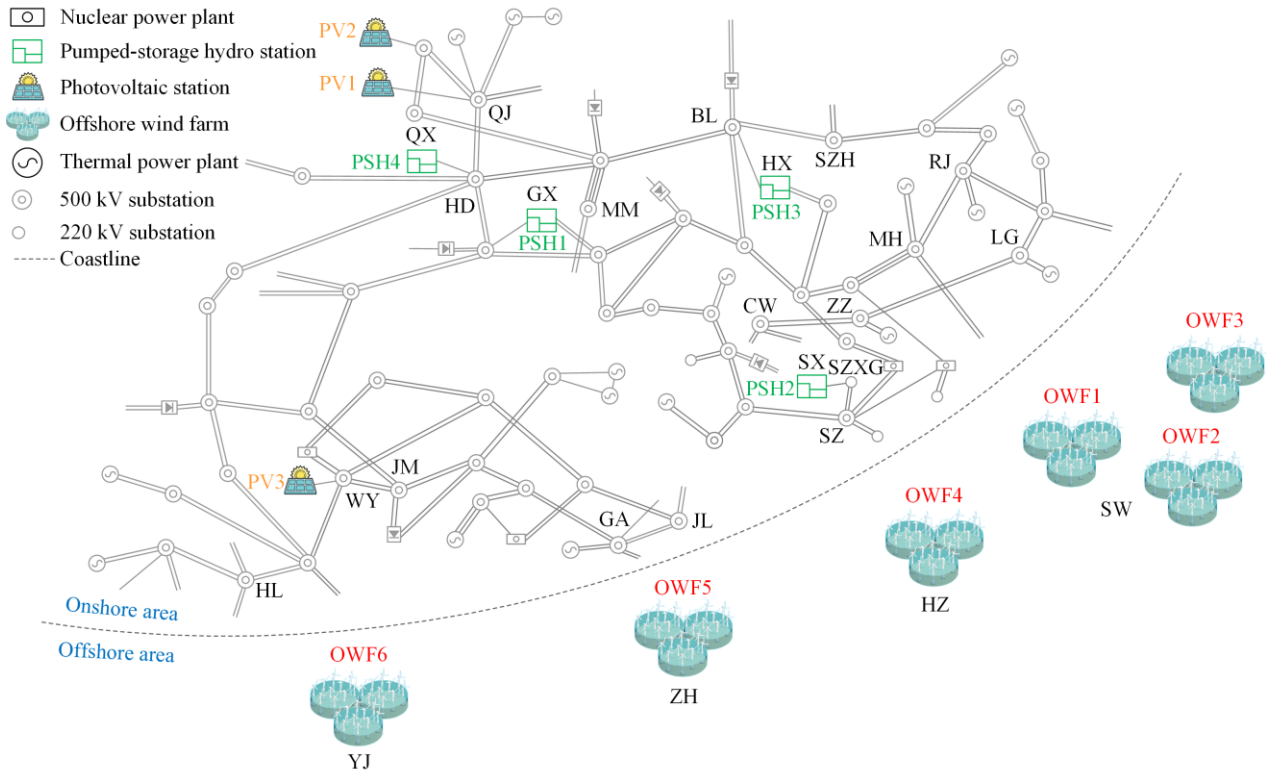

Fig. 8. Topology of the 500-kV main network of the provincial power grid.

TABLE III
PARAMETERS OF SIX OWFS TO BE PLANNED

OWF	Number of WTs	Rated power of each WT (MW)	Total capacity of OWF (MW)	Number of candidate PCCs	Transmission system mode
1	36	8	288	3	AC
2	78	6.45	503.1	3	VSC-MTDC
3	50	8	400	3	VSC-MTDC
4	40	6.25	250	3	AC
5	55	5.5	302.5	3	AC
6	73	5.5	401.5	3	VSC-MTDC

2) Analysis of Optimal Planning Results

By using the DCP algorithm to solve the proposed CP model, the optimal CP results are obtained as displayed in Tables IV and V. The optimal expansion planning scheme of the OTN is shown in Fig. 9. The optimal planning schemes of the six OWFs, along with the relative locations of the WTs, the candidate offshore/onshore substations and candidate PCCs of the six OWFs, are shown in Fig. 10, and the 500 kV substations near PCCs of each OWF in Fig. 10 can be correspondingly found in Fig. 9. For the expansion planning scheme of the OTN, six 500 kV lines near OWFs are newly built to transmit the large-scale offshore wind power to the OTN, and eight 220 kV lines are newly built to alleviate the line congestion problem caused by the load increase and ensure secure operation. For the planning schemes of INOWFs, with the influence of the power flow distribution in the OTN and different grid-connected positions of PCCs, the optimal planning schemes of the six OWFs present different characteristics. Due to the large number of WTs and large capacity of OWF2, two offshore substations and two PCCs are planned to make the wind power collection and transmission more distributed and improve the economics of planning, while the other five OWFs plan two offshore substations and one PCCs. Due to the large number and wide distribution range of WTs in OWF2, OWF5, and OWF6, two transmission submarine cables are planned to transmit wind power, while only one transmission submarine cable is planned in OWF1, OWF3, and OWF4. The topologies of the five OWFs except OWF4 adopt the new DSR with CSI, which improves the reliability of wind power integration and the power flow distribution within these OWFs, decreasing the power loss costs and making the wind curtailment costs zero. The results show that the proposed method can obtain the optimal CP scheme with great economics and reliability for multiple INOWFs and OTE.

TABLE IV
OPTIMAL PLANNING RESULTS OF THE OTN

Number of newly-built transmission lines	Annual equivalent investment cost (10^3¥)	Annual equivalent operation cost (10^3¥)	Total annual equivalent planning cost (10^3¥)
6 (500 kV)+ 8 (220 kV)	10 492.0	1 236 645.2	1 247 137.2

TABLE V
OPTIMAL PLANNING RESULTS OF OWFS

Item	OWF1	OWF2	OWF3	OWF4	OWF5	OWF6
Number of offshore/onshore substations	2/1	2/2	2/1	2/1	2/1	2/1
Number of PCCs	1	2	1	1	1	1
C_{in} (10^3¥)	246 068.7	538 547.6	466 484.7	245 864.0	250 272.4	379 888.9
C_{lo} (10^3¥)	160 97.6	54 130.3	39 003.4	18 727.6	21 335.3	56 025.8
C_{wc} (10^3¥)	0	0	0	0	0	0
f_{OWF} (10^3¥)	262 166.3	592 677.9	505 488.1	264 591.6	271 607.7	435 914.7

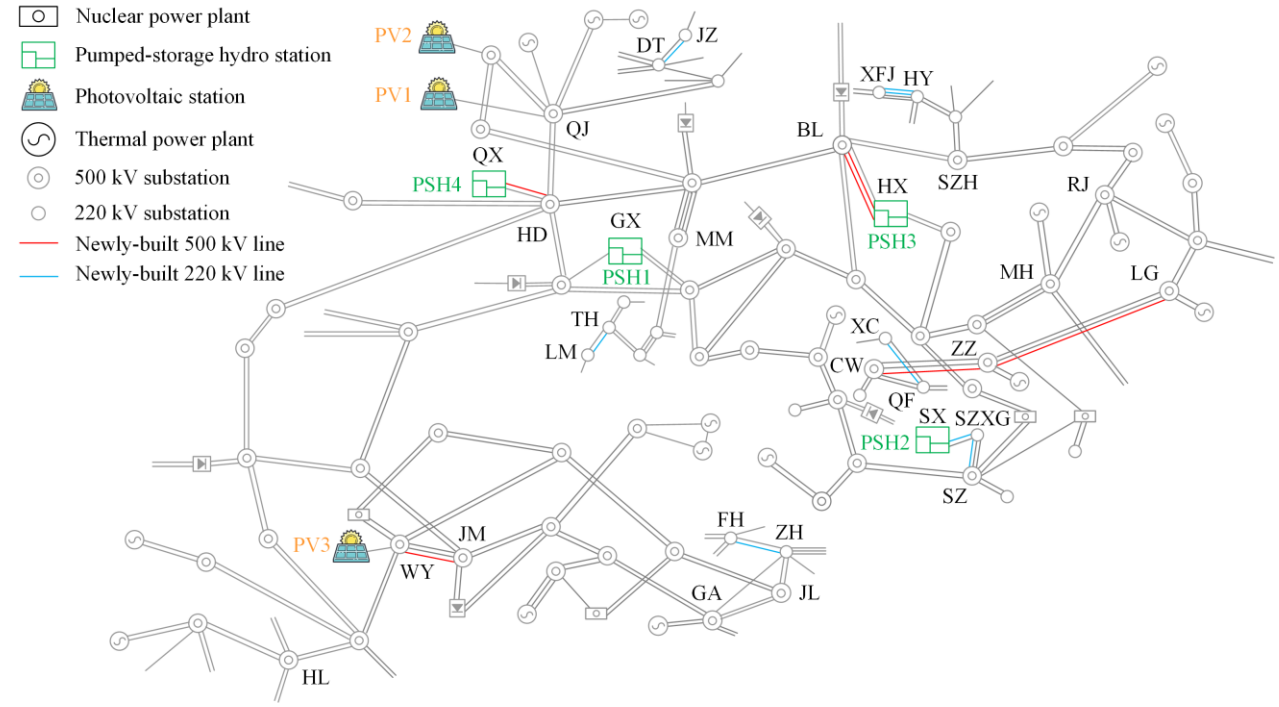

Fig. 9. Optimal expansion planning scheme of the OTN.

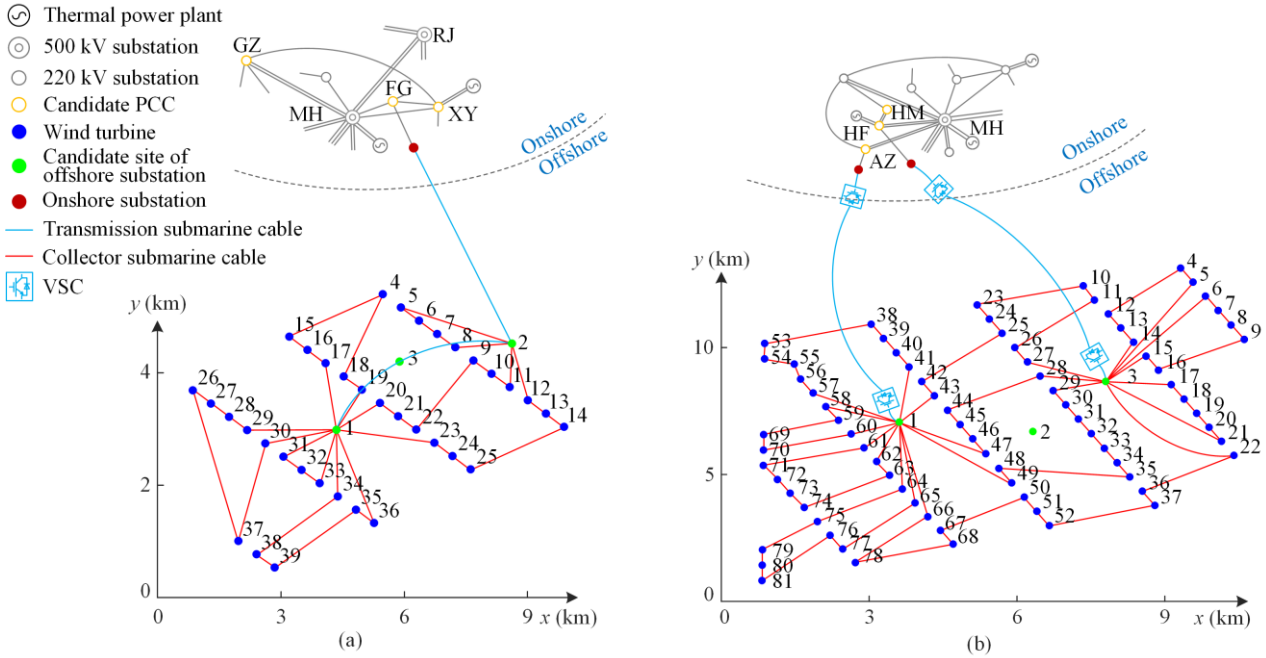

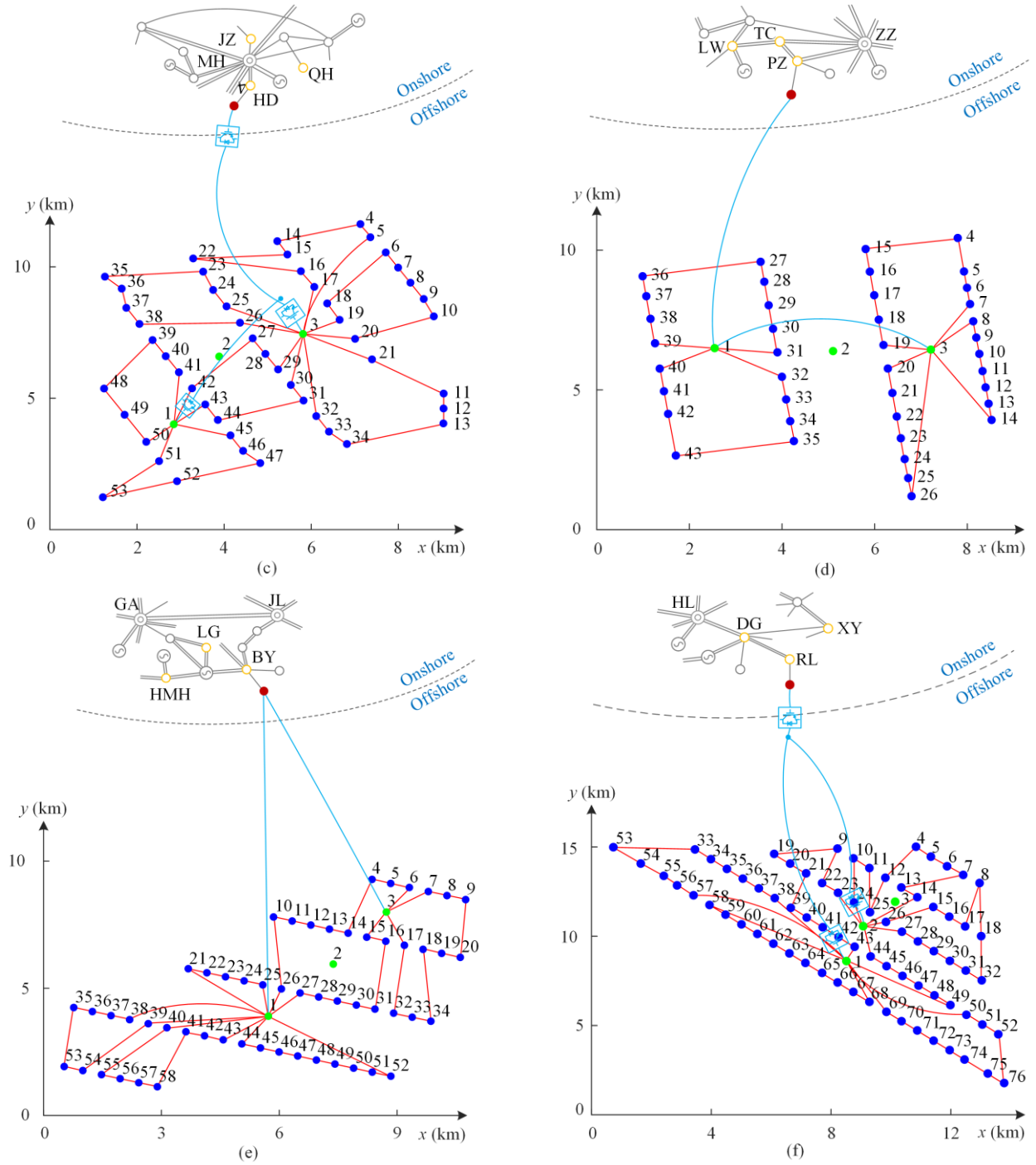

Fig. 10. Optimal planning schemes of six OWFs. (a) OWF1. (b) OWF2. (c) OWF3. (d) OWF4. (e) OWF5. (f) OWF6.

3) Comparison of Different Optimization Algorithms

For this actual large-scale power system with six OWFs to be planned, if the proposed PRS method is not used to constraint the feasible region, numerous binary variables and their possible combinations in the CP model will result in infeasible solution of the model. Comparative results of the algorithm in [21]–[26], the separated planning, centralized planning and proposed DCP algorithms using the proposed PRS method to constraint the feasible region are shown in Table VI. The sets Ω_{TC} of the PRS method for the last three algorithms are the same, and the consumed CPU time for parallel search of the feasible connection topology schemes is 3354 s. The algorithm in [21]–[26] ignores the impact of the INOWF planning on the OTE planning through PCCs, and cannot optimize the PCC locations. Thus, it results in poor economic benefits and its inability to obtain the optimal planning scheme of INOWFs corresponding to the obtained optimal OTE planning scheme. Since the intercoupling between the OTN and OWFs is ignored, the separated planning algorithm that solves the two planning sub-problems

separately has the shortest CPU time among the last three algorithms. But it cannot obtain the lowest overall planning cost, and the obtained solution lacks optimality. When the centralized planning algorithm is used to solve the CP model of the actual large-scale power system, the very large scale of the optimization model results in the high computational difficulty and low solution efficiency. Although the optimality gap is set to 6%, the centralized planning algorithm still requires 8237.2 s to obtain the optimal CP scheme, and the quality of the obtained optimal solution is poor with high total planning cost. In contrast, the proposed DCP algorithm has better convergence, the optimal CP scheme is obtained after 778.4 s and five alternating iterations among the two planning sub-problems, while the obtained solution has the lowest total planning cost. Thus, the results fully demonstrate the advantages of the proposed algorithm in solving the CP model of actual large-scale power systems with multiple OWFs.

TABLE VI
COMPARATIVE RESULTS OF DIFFERENT ALGORITHMS

Algorithm	f_{TE} (10^3¥)	f_{OWF} (10^3¥)	Total planning cost (10^3¥)	Optimality gap (%)	CPU time (s)
Algorithm in [21]–[26]	1 250 027.8			0.5	61.3
Separated planning with PRS	1 249 885.5	2 381 257.6	3 631 143.1	0.5	214.7
Centralized planning with PRS	1 250 382.9	2 442 393.1	3 692 776.0	6	8237.2
DCP with PRS	1 247 137.2	2 332 446.3	3 579 583.5	0.5	778.4

VI. CONCLUSIONS

In this paper, a CP model of multiple INOWFs and OTE is established. A PRS method for searching the feasible connection topology schemes of INOWFs and a DCP algorithm are proposed to efficiently solve the proposed CP model and obtain the optimal CP scheme. Case studies on the modified IEEE 39-bus system with two OWFs and an actual provincial power system with six OWFs demonstrate that the CP for the new DSR topologies in OWFs, the internal electrical components of INOWFs, and the onshore transmission corridor expansion can effectively reduce the wind power curtailment and load shedding while ensuring economic benefits. The proposed PRS method constraints the feasible region by searching the feasible connection topology schemes of INOWFs, and it can reduce the difficulty of obtaining the optimal solution. Compared with the separated and centralized planning algorithms, the proposed DCP algorithm can not only ensure the optimality of the obtained CP solution but also improve the solution efficiency.

With the increasing penetration of OWFs into power systems, enhancing the regulatory ability of the system to handle the power output fluctuation of OWFs and avoiding the risk of broadband oscillation of the system are highly important. Thus, the flexible reformation of conventional thermal units, the configuration of energy storages and the broadband oscillation suppression measures need to be further incorporated into the CP of multiple INOWFs and OTE, representing a potential direction of future work.

APPENDIX A

Parameters of different types of AC and DC submarine cables and transformers are listed in Tables AI–AIII. Parameters of PSH stations and PV stations in the actual provincial power system are listed in Table AIV.

TABLE AI
PARAMETERS OF DIFFERENT TYPES OF AC SUBMARINE CABLES

Type	Cross-sectional area (mm^2)	Current-carrying capacity (A)	Resistance (Ω/km)	Inductance (mH/km)
1	3×70	242	0.3420	0.3865
2	3×150	359	0.1587	0.3540
3	3×300	546	0.0778	0.3280

TABLE AII
PARAMETERS OF DIFFERENT TYPES OF DC SUBMARINE CABLES

Type	Rated capacity (MW)	Resistance (Ω/km)
1	500	0.0241
2	800	0.0224

TABLE AIII
PARAMETERS OF DIFFERENT TYPES OF TRANSFORMERS

Type	Rated capacity (MVA)
1	120
2	250
3	400

TABLE AIV
PARAMETERS OF PSH STATIONS AND PV STATIONS

		Maximum pumping power (MW)	Maximum generating power (MW)	Maximum stored energy (MWh)	Minimum generating power (MW)
PSH station	1	2400	2400	27 252	
	2	1200	1200	16 456	
	3	2400	2400	34 065	
	4	1280	1280	18 000	
PV station	1		450		0
	2		350		0
	3		400		0

ACKNOWLEDGMENT

Not applicable.

AUTHORS' CONTRIBUTIONS

Yutao Liang: case computation, writing, reviewing and editing. Shunjiang Lin: model and methodology construction, and supervision. Xin Lai: investigation. Mingbo Liu and Binrui Zhang: supervision. All authors read and approved the final manuscript.

FUNDING

This work is supported by the Guangdong Basic and Applied Basic Research Foundation (No. 2024B1515250007 and No. 2023A1515240075), and the Key Research and Development Project of Guangdong Province (No. 2021B0101230004).

AVAILABILITY OF DATA AND MATERIALS

Not applicable.

DECLARATIONS

Competing interests: The authors declare that they have no known competing financial interests or personal relationships that could have appeared to influence the work reported in this article.

AUTHORS' INFORMATION

Yutao Liang received the B.S. degree in electrical engineering from the South China University of Technology, in 2022. He is currently pursuing the M.S. degree with the School of Electric Power Engineering, South China University of Technology. His research interests include power system planning, optimization, operation, and control.

Shunjiang Lin received the B.S. degree in electrical engineering from South China University of Technology, in 2003, and the Ph.D. degree in electrical engineering from Hunan University, in 2008. He is currently an associate professor with the School of Electric Power Engineering, South China University of Technology. His research interests include power system optimization, operation and control.

Xin Lai received the B.S. degree in electrical engineering from the South China University of Technology, in 2023. He is currently pursuing the M.S. degree with the School of Electric Power Engineering, South China University of Technology. His research interests include power system optimization, operation, and control.

Mingbo Liu received the B.S. degree from the Huazhong University of Science and Technology, in 1985, the M.S. degree from the Harbin Institute of Technology, in 1988, and the Ph.D. degree from Tsinghua University, in 1992. He is currently a professor with the South China University of Technology. He has authored and coauthored four monographs, two standards, and more than 280 articles. His research interests include energy management and operation control of power systems.

Binrui Zhang received the M.S. degree from the Harbin Institute of Technology, in 2009. He is currently an engineer from China Nuclear Power Engineering Co., Ltd., and engaged in technical management of offshore wind power engineering.

REFERENCES

[1] H. Díaz and C. G. Soares, "Review of the current status, technology and future trends of offshore wind farms," *Ocean Engineering*, vol. 209, Jun. 2020.

[2] G. Abeynayake, T. Van Acker, and D. V. Hertem *et al.*, "Analytical model for availability assessment of large-scale offshore wind farms including their collector system," *IEEE Transactions on Sustainable Energy*, vol. 12, no. 4, pp. 1974-1983, Oct. 2021.

[3] R. Lu, X. Xiong, and H. Chen, "Collaborative emergency defense strategy for offshore wind farm clusters considering the spatial-temporal characteristics of a typhoon," *Power System Protection and Control*, vol. 52, no. 12, pp. 13-24, Jun. 2024. (in Chinese)

[4] P. Lakshmanan, R. Sun, and J. Liang, "Electrical collection systems for offshore wind farms: a review," *CSEE Journal of Power and Energy Systems*, vol. 7, no. 5, pp. 1078-1092, Sept. 2021.

[5] Y. Liu, Y. Fu, and L. Huang *et al.*, "Optimization of offshore grid planning considering onshore network expansions," *Renewable Energy*, vol. 181, pp. 91-104, Jan. 2022.

[6] Y. K. Wu, P. E. Su, and Y. S. Su *et al.*, "Economics-and reliability-based design for an offshore wind farm," *IEEE Transactions on Industry Applications*, vol. 53, no. 6, pp. 5139-5149, Nov. 2017.

[7] S. Tao, Q. Xu, and A. Feijóo *et al.*, "Joint optimization of wind turbine micrositing and cabling in an offshore wind farm," *IEEE Transactions on Smart Grid*, vol. 12, no. 1, pp. 834-844, Jan. 2021.

[8] O. Dahmani, S. Bourguet, and M. Machmoum *et al.*, "Optimization and reliability evaluation of an offshore wind farm architecture," *IEEE Transactions on Sustainable Energy*, vol. 8, no. 2, pp. 542-550, Apr. 2017.

[9] S. Wei, L. Zhang, and Y. Xu *et al.*, "Hierarchical optimization for the double-sided ring structure of the collector system planning of large offshore wind farms," *IEEE Transactions on Sustainable Energy*, vol. 8, no. 3, pp. 1029-1039, Jul. 2017.

[10] X. Shen, Q. Wu, and H. Zhang *et al.*, "Optimal planning for electrical collector system of offshore wind farm with double-sided ring topology," *IEEE Transactions on Sustainable Energy*, vol. 14, no. 3, pp. 1624-1633, Jul. 2023.

[11] J. Dakic, M. Cheah-Mane, and O. Gomis-Bellmunt *et al.*, "HVAC transmission system for offshore wind power plants including mid-cable reactive power compensation: optimal design and comparison to VSC-HVDC transmission," *IEEE Transactions on Power Delivery*, vol. 36, no. 5, pp. 2814-2824, Oct. 2021.

[12] K. Meng, W. Zhang, and J. Qiu *et al.*, "Offshore transmission network planning for wind integration considering AC and DC transmission options," *IEEE Transactions on Power Systems*, vol. 34, no. 6, pp. 4258-4268, Nov. 2019.

[13] S. Paul and Z. H. Rather, "A novel approach for optimal cabling and determination of suitable topology of

MTDC connected offshore wind farm cluster," *Electric Power Systems Research*, vol. 208, Jul. 2022.

[14] T. Zuo, Y. Zhang, and K. Meng *et al.*, "Collector system topology for large-scale offshore wind farms considering cross-substation incorporation," *IEEE Transactions on Sustainable Energy*, vol. 11, no. 3, pp. 1601-1611, Jul. 2020.

[15] E. Taherzadeh, H. Radmanesh, and S. Javadi *et al.*, "Circuit breakers in HVDC systems: state-of-the-art review and future trends," *Protection and Control of Modern Power Systems*, vol. 8, no. 3, pp. 1-16, Jul. 2023.

[16] K. Henrik and O. T. John, "The NOWITECH reference wind farm," *Energy Procedia*, vol. 53, pp. 300-312, 2014.

[17] Y. Li, X. Qiao, and C. Chen *et al.*, "Integrated optimal siting and sizing for VSC-HVDC-link-based offshore wind farms and shunt capacitors," *Journal of Modern Power Systems and Clean Energy*, vol. 9, no. 2, pp. 274-284, Mar. 2021.

[18] L. Baringo and A. Baringo, "A stochastic adaptive robust optimization approach for the generation and transmission expansion planning," *IEEE Transactions on Power Systems*, vol. 33, no. 1, pp. 792-802, Jan. 2018.

[19] J. Li, Z. Li, and F. Liu *et al.*, "Robust coordinated transmission and generation expansion planning considering ramping requirements and construction periods," *IEEE Transactions on Power Systems*, vol. 33, no. 1, pp. 268-280, Jan. 2018.

[20] Z. Zhou, C. He, and T. Liu *et al.*, "Reliability-constrained AC power flow-based co-optimization planning of generation and transmission systems with uncertainties," *IEEE Access*, vol. 8, pp. 194218-194227, Oct. 2020.

[21] L. Gan, G. Li, and M. Zhou, "Coordinated planning of large-scale wind farm integration system and transmission network," *CSEE Journal of Power and Energy Systems*, vol. 2, no. 1, pp. 19-29, Mar. 2016.

[22] C. Zhang, H. Cheng, and L. Liu *et al.*, "Coordination planning of wind farm, energy storage and transmission network with high-penetration renewable energy," *International Journal of Electrical Power & Energy Systems*, vol. 120, Sept. 2020.

[23] Q. Li, J. Wang, and Y. Zhang *et al.*, "Hierarchical market-based optimal planning of transmission network and wind-storage hybrid power plant," *International Journal of Electrical Power & Energy Systems*, vol. 153, Nov. 2023.

[24] S. Dehghan, N. Amjady, and P. Aristidou, "A robust coordinated expansion planning model for wind farm-integrated power systems with flexibility sources using affine policies," *IEEE Systems Journal*, vol. 14, no. 3, pp. 4110-4118, Sept. 2020.

[25] K.A. Alnowibet, A.F. Alrasheedi, and A.M. Alshamrani, "Integrated stochastic transmission network and wind farm investment considering maximum allowable capacity," *Electric Power Systems Research*, vol. 215, Feb. 2023.

[26] M. Taherkhani, S. H. Hosseini, and M. S. Javadi *et al.*, "Scenario-based probabilistic multi-stage optimization for transmission expansion planning incorporating wind generation integration," *Electric Power Systems Research*, vol. 189, Dec. 2020.

[27] Y. Liang, S. Lin, and X. Feng *et al.*, "Optimal resilience enhancement dispatch of a power system with multiple offshore wind farms considering uncertain typhoon parameters," *International Journal of Electrical Power & Energy Systems*, vol. 153, Nov. 2023.

[28] M. Dicorato, G. Forte, and M. Pisani *et al.*, "Guidelines for assessment of investment cost for offshore wind generation," *Renewable Energy*, vol. 36, no. 8, pp. 2043-2051, Aug. 2011.

[29] J. Yang, N. Zhang, and C. Kang *et al.*, "A state-independent linear power flow model with accurate estimation of voltage magnitude," *IEEE Transactions on Power Systems*, vol. 32, no. 5, pp. 3607-3617, Sept. 2017.

[30] A. R. L. Oliveira, S. Soares, and L. Nepomuceno, "Optimal active power dispatch combining network flow and interior point approaches," *IEEE Transactions on Power Systems*, vol. 18, no. 4, pp. 1235-1240, Nov. 2003.

[31] J. Yang, J. O'Reilly, and J. E. Fletcher, "Redundancy analysis of offshore wind farm collection and transmission systems," in *2009 International Conference on Sustainable Power Generation and Supply*, Nanjing, China, Apr. 2009, pp. 1-7.

[32] X. Feng, S. Lin, and W. Liu *et al.*, "Distributionally robust optimal dispatch of offshore wind farm cluster connected by VSC-MTDC considering wind speed correlation," *CSEE Journal of Power and Energy Systems*, vol. 9, no. 3, pp. 1021-1035, May 2023.